Some mechanistic underpinnings of molecular adaptations of SARS-COV-2 spike protein by integrating candidate adaptive polymorphisms with protein dynamics

Nicholas J. Ose[1], Paul Campitelli[1], Tushar Modi[1], I. Can Kazan[1], Sudhir Kumar[2,3,4,*] and S. Banu Ozkan[1,*]

[1]Department of Physics and Center for Biological Physics, Arizona State University, Tempe, Arizona, United States of America

[2]Institute for Genomics and Evolutionary Medicine, Temple University, Philadelphia, Pennsylvania, United States of America

[3]Department of Biology, Temple University, Philadelphia, Pennsylvania, United States of America

[4]Center for Genomic Medicine Research, King Abdulaziz University, Jeddah, Saudi Arabia

* s.kumar@temple.edu (SK); * Banu.Ozkan@asu.edu (SBO)

Abstract

We integrate evolutionary predictions based on the neutral theory of molecular evolution with protein dynamics to generate mechanistic insight into the molecular adaptations of the SARS-COV-2 Spike (S) protein. With this approach, we first identified Candidate Adaptive Polymorphisms (CAPs) of the SARS-CoV-2 Spike protein and assessed the impact of these CAPs through dynamics analysis. Not only have we found that CAPs frequently overlap with well-known functional sites, but also, using several different dynamics-based metrics, we reveal the critical allosteric interplay between SARS-CoV-2 CAPs and the S protein binding sites with the human ACE2 (hACE2) protein. CAPs interact far differently with the hACE2 binding site residues in the open conformation of S protein compared to the closed form. In particular, the CAP sites control the dynamics binding residues in the open state, suggesting an allosteric control of hACE2 binding. We also explored the characteristic mutations of different SARS-CoV-2 strains to find dynamic hallmarks and potential effects of future mutations. Our analyses reveal that Delta strain-specific variants have non-additive (i.e., epistatic) interactions with CAP sites, whereas the less pathogenic Omicron strains have mostly compensatory variants. Finally, our dynamics-based analysis suggests that the novel mutations observed in the Omicron strain epistatically interact with the CAP sites to help escape antibody binding.

Introduction

Since 2019, the evolution of SARS-CoV-2 in humans has been characterized by the spread of mutations, many notably found within the Spike (S) glycoprotein. The S protein is directly related to the human immune response to COVID-19 and, as such, has been one of the most studied and targeted proteins in the SARS-CoV-2 research (Shang et al. 2020; Harvey, Carabelli, Jackson, Gupta, Thomson, Harrison, Ludden, Reeve, Rambaut, Consortium, et al. 2021; Jackson et al. 2022; Carabelli et al. 2023; Markov et al. 2023). Subsequently, research into the biophysical properties and mutational patterns associated with S

41 protein evolution not only remains critical to understanding the pandemic but also emerges as a useful
42 system to understand the mechanics of molecular adaptation within viruses.

43 For successful infection of a human host, the S glycoprotein of SARS-CoV-2 binds to the human ACE2
44 (hACE2) receptor through its receptor-binding domain (RBD). Evidence indicates that fine-tuning S protein
45 interactions with hACE2 significantly affects viral reproduction (Rehman et al. 2020; Saputri et al. 2020;
46 Rochman et al. 2021). Previous evolutionary studies show a complex network of interactions among
47 mutated residues (Changeux and Edelstein 2005; Doshi et al. 2016; O'Rourke et al. 2016; Mishra and
48 Jernigan 2018). Therefore, there has been a vast effort to uncover which mutations are important steps
49 of adaptation for the S protein (Cagliani et al. 2020; Damas et al. 2020; Singh and Yi 2021; Kistler et al.
50 2022; Maher et al. 2022; Neher 2022). In particular, a significant aspect of many such studies was a focus
51 on understanding adaptive mutations of SARS-CoV-2 that contributed to the leap to human hosts (Cagliani
52 et al. 2020; Damas et al. 2020; Singh and Yi 2021; Starr, Zepeda, et al. 2022). This is because SARS-CoV-2
53 has continuously mutated since its early detection (Kistler et al. 2022), causing the emergence of CDC-
54 designated "variants of concern" (VOCs) that an accelerated substitution rate may drive (Tay et al. 2022).

55 Predicting how new mutations impact the biophysical properties of the S protein remains a challenge, let
56 alone explaining their complex interactions with one-another and how they might affect hACE2 binding
57 because many factors affect hACE2 interactions. Binding affinity with hACE2 can be enhanced directly
58 through stronger receptor interactions or mediated through changes in RBD opening (Teruel et al. 2021;
59 Zhang et al. 2021; Díaz-Salinas et al. 2022). The RBD exhibits both 'closed' and 'open' conformational
60 states. In the closed state, the RBD is shielded from receptor binding. In the open state, the RBD is
61 accessible for hACE2 binding (Kirchdoerfer et al. 2016; Gur et al. 2020; Henderson et al. 2020; Hoffmann
62 et al. 2020). While some mutations may affect the transition between these states (Henderson et al. 2020;
63 Yurkovetskiy et al. 2020; Gobeil, Janowska, McDowell, Mansouri, Parks, Manne, et al. 2021; Sztain et al.
64 2021; Zhang et al. 2021; Shoemark et al. 2022), the other mutations may allosterically regulate RBD

65 openings through Furin cleavage site (residue ID range: 681-695) interactions to regulate hACE2 binding
66 (Deng et al. 2021; Gobeil, Janowska, McDowell, Mansouri, Parks, Stalls, et al. 2021; Khan et al. 2021;
67 Laiton-Donato et al. 2021).

68 Moreover, as new mutations accumulate, culminating in the emergence of a new VOC, these mutations
69 must occur on varied sequence backgrounds containing neutral, nearly-neutral, and adaptive mutations.
70 While many studies have explored the impacts of individual mutations, VOCs result in a substantial
71 difference in protein function compared to their individual effects (Moulana et al. 2022a; Starr, Greaney,
72 Hannon, et al. 2022; Moulana et al. 2023; Witte et al. 2023). Here we integrate an evolutionary approach
73 with protein dynamics analysis to address the fundamental mechanisms of mutations dictating the VOCs
74 and the impact of their epistatic interaction on the function of the S protein. Many earlier studies have
75 combined phylogeny and evolutionary theory to identify adaptive mutations as well as to see how the
76 viral sequence has changed over time (Frost et al. 2018; Boni et al. 2020; Cagliani et al. 2020; Damas et al.
77 2020; Tang et al. 2020). Similarly, we first use a well-established Evolutionary Probability (EP) approach
78 (Liu et al. 2016) that utilizes phylogenetic trees in combination with the neutral theory of molecular
79 evolution to determine Candidate Adaptive Polymorphisms (CAPs) determined using the early Wuhan
80 sequence as a variant. CAPs are substitutions in SARS-CoV-2 that are rarely observed in other closely
81 related sequences (Figure 1A), which implies a degree of functional importance and makes them
82 candidates for adaptation (Liu et al. 2016). In support of this method, we find an overlap between our list
83 of sites containing CAPs and putative adaptive sites identified by others (Cagliani et al. 2020; Singh and Yi
84 2021; Starr, Zepeda, et al. 2022). Second, we use a suite of computational tools to analyze how CAPs that
85 arose in the early and late phases of the COVID-19 pandemic modulate the dynamics of the S protein. We
86 also explore the complex interactions between these sets of CAPs to gain mechanistic insight into the
87 behavior of molecular adaptation involving the S protein. In particular, we focused on how mutations
88 modulate protein dynamics, as we and others have previously found that rather than changing a protein's

89 structure solely, mutations modulate conformational dynamics leading to changes in biophysical
90 properties such as stability, flexibility, and allosteric dynamic coupling, any of which may affect protein
91 binding (Swint-Kruse et al. 1998; Keskin et al. 2000; Bhabha et al. 2013; Nussinov, R., Tsai, C.-J 2013;
92 Campbell, E. et al. 2016; Ma and Nussinov 2016: 201; Saavedra et al. 2018; Kuzmanic et al. 2020).

93 With this evolutionary-dynamics unified approach, we aim to answer the following questions about VOCs:
94 Are all the mutations in VOCs adaptive in nature? Are they coupled to one another or provide some
95 measure of biophysical, dynamical, or mechanical compensation? While many of these mutations are
96 found within the RBD domain, numerous others are located distal to this region; hence, we aim to
97 investigate the functional roles of distal mutations, particularly from a protein dynamics perspective. Our
98 integrated analysis revealed that protein dynamics play a significant role in the evolution of the S protein.
99 The flexibility of sites withing the S protein shows a strong, direct correlation with substitution rate, and
100 newly evolving CAPS are mostly compensatory (i.e., additive) mutations that modulate the dynamics of
101 the hACE2 binding site. Yet other CAPs, 346R, 486F, and 498Q, show highly epistatic (i.e., non-additive)
102 modulation of the hACE2 binding site and provide immune escape benefits.

103

104 **Results and Discussions**

105 **Candidate Adaptive mutations in the Spike protein are recognized via Evolutionary Probabilities.**

106 SARS-CoV-2 is part of a family of coronaviruses, many of which infect mainly animals and are less capable
107 of infecting humans (Dicken et al. 2021). Therefore, to identify the most likely mutations responsible for
108 the infection of human hosts (i.e., putative adaptive mutations for humans), we estimated the (neutral)
109 evolutionary probability (EP) scores of mutations found within the S protein (Liu et al. 2016). EP scores of
110 the amino acid variants of S protein are obtained by constructing a maximum likelihood phylogenetic tree
111 (Goldman 1990) containing 19 orthologous coronavirus sequences, which were selected based on the

112 amount of divergence over evolutionary history to ensure that each amino acid position had ample time
113 to experience purifying selection (Patel et al. 2018) (Figure 1A). The likelihood of finding a particular amino
114 acid in the sequence is then determined using a Bayesian framework, with calculations carried out by
115 MEGA X software (Kumar et al. 2018). As apparent in the name, EP scores obtained for the amino acids in
116 the sequence provide information regarding the likelihood of finding them at their position, given the
117 history of the sequence. Amino acid residues receiving low EP scores (<0.05) at a position are less likely to
118 be found in a given position within the sequence because they are non-neutral. Generally, positions with
119 low EP amino acids are far less common than those containing mutations with high EP, a trend also
120 realized in the CoV-2 S protein (Figure 1B).

121 Of particular interest is an observed evolutionary change where an amino acid with high EP is replaced by
122 an amino acid residue with low EP. While amino acids with low EP should be harmful or deleterious to
123 viral fitness due to functional disruption or change, fixation of a low EP amino acid at a position suggests
124 an underlying mechanism for natural selection to operate. These fixed, low EP mutations are called
125 candidate adaptive polymorphisms (CAPs) as they are predicted to alter protein function, and adaptive
126 pressures may drive their prevalence (Patel et al. 2018). Indeed, there is an overlap between these CAPs
127 and the mutations suggested by other methods to be adaptive for the S protein (Cagliani et al. 2020; Singh
128 and Yi 2021; Starr, Zepeda, et al. 2022).

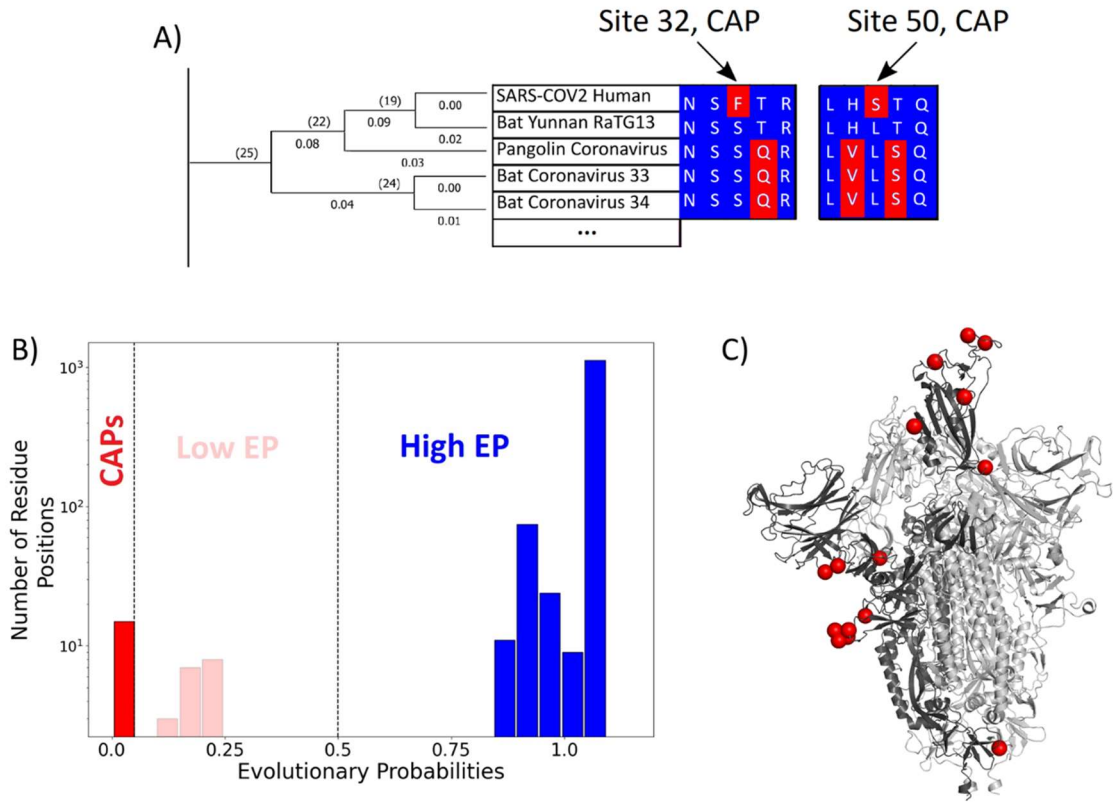

Figure 1. (A) The evolutionary probabilities (EP) of each amino acid in the S protein sequence are calculated by taking the multiple sequence alignment of the S proteins through their evolutionary tree and using Bayesian inferences to determine the likelihood of finding a particular residue at a particular location within a given sequence. Simply, if the residue is found at a location 'x' in closely related sequences, it will have a higher EP at location 'x' in the target sequence. Residues with an EP <0.05 in the target sequence are CAPs (Red). (B) The distribution of EP scores of the wild-type residues in the S protein. Here, lower EP scores are shown in red, and higher EP scores in blue. While the vast majority of the wild-type (reference) protein consists of high EP residues, a few residues have low EP. (C) The CAPs are also highlighted as red spheres in the open configuration of the S protein, with the open chain in a darker shade. We observe that a majority of the CAP positions reside at the receptor binding domain (RBD) and the Furin cleavage site (676-689; (Wrobel et al. 2020)) shown as transparent light gray spheres.

Interestingly, most of the CAP residues are in functionally critical sites, including the receptor binding domain (RBD) and the Furin cleavage site (Figure 1C). As mentioned earlier, the RBD plays a key role in initiating the infection of a healthy cell by binding it with the host organism's ACE2 protein. Before ACE2

144 binding, one chain of the homotrimer comprising the S protein must open to expose the RBD (Kirchdoerfer
145 et al. 2016; Henderson et al. 2020; Hoffmann et al. 2020; Sztain et al. 2021). The Furin cleavage site plays
146 a key role in the opening process as it aids in the cleavage of the S protein into two domains: S1 and S2
147 (Wrobel et al. 2020: 13). Similar cleavage sites have been found in related coronaviruses, including HKU1
148 and Middle East respiratory syndrome coronavirus (MERS-CoV), which infect humans (Chan et al. 2008:
149 1; Millet and Whittaker 2014; Millet and Whittaker 2015), and the acquisition of similar cleavage sites is
150 associated with increased pathogenicity in other viruses such as the influenza virus (Steinhauer 1999).
151 Interestingly, however, CAPs do not display such an overwhelming tendency to occur at well-known
152 critical sites within human proteins studied with similar methods (Ose, Campitelli, et al. 2022), yet
153 mutations at those sites are associated with disease, indicating their critical role in inducing functional
154 change. Therefore, the identified CAPs in the S protein, which are signs of recent evolution, can provide
155 mechanistic insights regarding the molecular adaptation of the virus. In particular, we aimed to analyze
156 how these CAP positions in the S protein modulate the interaction with hACE2 using our protein dynamics-
157 based analysis (Gerek and Ozkan 2011; Nevin Gerek, Z., Kumar, S., Banu Ozkan, S. 2013; Larrimore et al.
158 2017; Kumar, A., Glembo, T.J., Ozkan, S.B. 2015b).

159

160 **Asymmetry in communications among the network of interactions in Spike describes how CAPs regulate**
161 **the dynamics of the Spike protein.**

162 A mutation at a given amino acid position inevitably not only alters local interactions, but this change
163 cascades through the residue-residue interaction network, which gives rise to a variation in native
164 ensemble dynamics to modulate function (Dror et al. 2012; Labbadia and Morimoto 2015; Sekhar and Kay
165 2019; Campitelli et al.). Thus, we analyze the internal dynamics of the system to understand the functional
166 role of CAPs in S proteins. This analysis allows us to gain a mechanistic understanding of the relationship

167 between CAP mutations and biophysical outcomes (Teruel et al. 2021). First, we implement the Dynamic
168 Coupling Index (DCI) approach to study long-distance coupling between the CAPs and the hACE2 binding
169 sites emerging from the 3D network of interactions across the S protein system. The DCI parameter
170 combines Perturbation Response Scanning and Linear Response Theory to capture the strength of a
171 displacement response for position *i* upon perturbation of position *j*, relative to the average fluctuation
172 response of position *i* to all other positions in the protein. It represents the strength of dynamic coupling
173 between positions *i* and *j* upon perturbation to *j.*

174 Further, asymmetry can be captured in the DCI values, as dynamic coupling is not necessarily due to an
175 anisotropic network. That is, each amino acid has a set of positions to which it is highly coupled, and this
176 anisotropy in connections gives rise to unique differences in coupling between a given *i, j* pair of amino
177 acids which do not have direct interactions. By calculating the coupling of the hACE2 binding interface in
178 the RBD with respect to the CAP residue positions and vice versa, we can generate DCI_{asym} (Figure 2A) as
179 the difference between the normalized displacement response of position *j* upon a perturbation to
180 position *i* (DCI_{ij}) and the normalized displacement response of position *i* upon a perturbation to position *j*
181 (DCI_{ji}) (See Methods). If the DCI_{asym} values significantly differ from zero, it shows asymmetry in coupling
182 and presents a cause-effect relationship between the *i, j* pair in terms of force/signal propagation. This
183 metric has been used previously in a variety of systems to analyze the unique behavior of positions within
184 a protein and a given position's propensity to effect biophysical changes upon mutation, particularly at
185 long distances (Modi and Ozkan 2018; Campitelli and Ozkan 2020; Kolbaba-Kartchner et al. 2021; Ose,
186 Butler, et al. 2022; Kazan et al. 2023; Campitelli et al. 2020b).

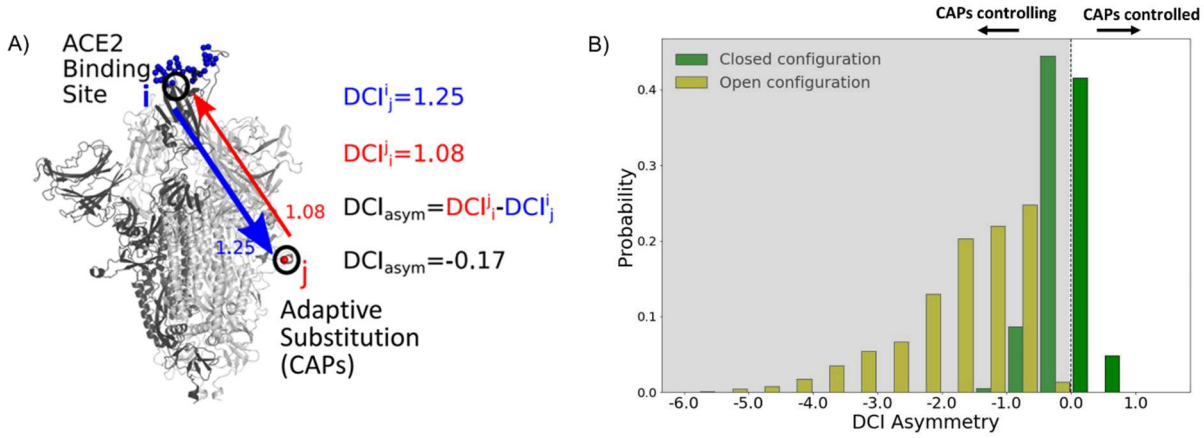

Figure 2. (A) Schematic representation of DCI asymmetry. (B) DCI asymmetry of CAP residue positions with the binding interface of RBD in the open chain. Residues in the closed chains with a low EP amino acid in the reference sequence dominate the binding site interface of RBD in the open chain. There is a significant difference between the asymmetry profiles of the closed (M = -0.06, SD = 0.33) and open (M = -1.68, SD = 0.89) conformations ($p < .001$).

Recent work from our group has shown an enhancement in cross-chain communication within the main protease of SARS COV-2 compared to SARS COV-1 (Campitelli et al. 2022). Furthermore, previous studies have shown that allosteric inter-chain communication is important to S protein function (Zhou et al. 2020; Spinello et al. 2021; Tan et al. 2022; Xue et al. 2022). In support of these findings, we observe through DCI_{asym} that when the S protein is in its pre-fusion conformation with one chain open, the CAPs in the closed chains have negative coupling asymmetry with respect to the hACE2 binding site interface in the RBD-open chain. This indicates an allosteric control where the hACE2 binding site is dominated by the dynamics of the CAPs in closed chains (Figure 2B, yellow bars). As this open-state RBD is critical for the viral infection of host cells (Kirchdoerfer et al. 2016), our results suggest that this type of closed-to-open cross-chain interaction is important for viral proliferation. Our prior studies on DCI_{asym} show a similar trend in Lactose Inhibitor (LacI), a protein with a functional role in gene expression through binding DNA. The allosteric mutations (i.e., mutations on the sites that are far from the DNA binding sites) that alter DNA

206 binding affinity not only exhibited unique asymmetry profiles with the DNA binding sites of LacI, but also
207 regulated the dynamics of these binding sites (Campitelli et al. 2020b).

208 Similarly, it is possible that mutations to such residue positions within the S protein can be used to regulate
209 the dynamics of the hACE2 bindings sites of the open RBD state. We, therefore, propose that the residue
210 positions with CAP substitutions hold the potential for mutations in the spike sequence which can alter
211 the opening and closing dynamics of the RBD domain. This hypothesis is further supported by many
212 mutations already observed at these residue positions which alter the infection rate (Brister et al. 2015).
213 Interestingly, residues responsible for extremely low asymmetry values (< -4) lie overwhelmingly in the
214 region 476–486. These same residues were suggested to stabilize S protein dynamics and prime it for host
215 Furin proteolysis (Raghuvamsi et al. 2021).

216 Moreover, as a control, we performed the same analysis on the S protein with the RBD domains of all
217 chains in the closed configuration. In this case, we observed that the DCI_{asym} of the CAPs residue positions
218 with respect to the hACE2 interface in the other chains yields a largely symmetric distribution about 0
219 (Figure 2B, green bars). This verifies that the asymmetry in the coupling of CAPs with the exposed binding
220 site interface in pre-fusion configuration results from one of the RBDs opening up and further suggests
221 the allosteric role played by CAPs in locking the S protein in the RBD open state.

222

223 **Dynamic analysis shows that rigid sites tend to be more highly conserved than flexible sites.**

224 CAPs represent important S protein amino acid changes between related coronaviruses across multiple
225 species and the Wuhan-Hu-1 reference sequence (MN908947). Since SARS-CoV-2 first spread to humans,
226 it has continued to mutate and evolve rapidly, particularly regarding the S protein (Amicone et al. 2022;
227 Liu et al. 2022; Tay et al. 2022). Like the mutations leading to the Wuhan strain caused an increase in
228 binding affinity to hACE2, continued evolution in human hosts has resulted in further altered binding

229 affinities as well as different phenotypic outcomes for those infected (Ali et al. 2021; Barton et al. 2021;
230 Ozono et al. 2021).

231 We explore whether protein dynamics has played a role in the selection of mutational sites during the
232 evolution of the S protein since 2019. Our previous work has indicated that rate of evolution per positional
233 site exhibits a positive correlation with positional flexibility; generally, positions that exhibit higher
234 flexibility are also sites that experience a higher number of amino acid substitutions (Liu and Bahar 2012;
235 Maguid et al. 2008; Maguid et al. 2006; Mikulska-Ruminska et al. 2019; Nevin Gerek, Z., Kumar, S., Banu
236 Ozkan, S. 2013). To confirm these findings for the evolution of the S protein using the sequenced variants
237 of infected humans, we analyze the site-specific amino acid flexibility using the Dynamic Flexibility Index
238 (DFI). Using the same mathematical foundation as DCI, DFI evaluates each position's displacement
239 response to random force perturbations at other locations in the protein (Gerek and Ozkan 2011; Nevin
240 Gerek, Z., Kumar, S., Banu Ozkan, S. 2013), and it can be considered a measure of a given position's ability
241 to explore its local conformational space. We found that the covid-19 S protein shows the expected high
242 correlation between the occurrence of mutations and site flexibility (Figure 3) when we compare %DFI
243 (DFI ranked by percentile) to the average number of variants per position found within a given %DFI bin.
244 Previous studies have indicated that rigid residues are critical for functional dynamics, thus more likely to
245 impact function if mutated and, generally, can lead to a loss of function and thus more conserved (Kim,
246 H. et al. 2015; Butler et al. 2018; Modi, Risso, et al. 2021; Modi, Campitelli, et al. 2021; Kazan et al. 2022;
247 Ose, Butler, et al. 2022; Stevens et al. 2022; Campitelli et al. 2020a; Kumar, A., Glembo, T.J., Ozkan, S.B.
248 2015b). This analysis also agrees with these previous studies and highlights the power of negative
249 selection, in line with the neutral theory of molecular evolution, stating that deleterious mutations (i.e.,
250 those on the rigid positions) should be eliminated and therefore not observed (Kimura, Motoo 1983).

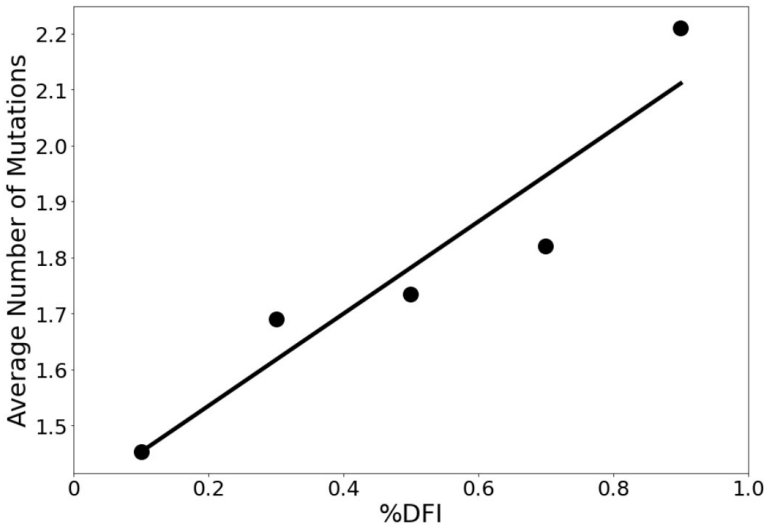

Figure 3. The average number of variants observed among residues of different flexibility. Residues were sorted into one of five bins based on flexibility. After that, the average number of variants for residues within that bin was calculated. Here, the number of variants is defined as the number of different amino acid varieties found at that site. Mutational data was calculated across approximately 24,000 SARS-CoV-2 S protein sequences from the NCBI Datasets Project (Brister et al. 2015). Residue flexibility, as reported here via %DFI, was computed using structure id 6vsb from the Protein DataBank (Berman, H.M. et al. 2000). More rigid residues tend to have fewer variants. (r = 0.94).

Continued mutations within human hosts have resulted in a multitude of variants. Indeed, by fitting various molecular clock models to genome sequence data, VOC emergence is punctuated by an episodic period of rapid evolution, with a substitution rate of up to 4-fold greater than the background substitution rate (Kumar et al. 2021; Tay et al. 2022). With such an aggressive evolutionary rate, we are finding VOCs to consist of a number of different characteristic mutations, almost all of which are CAPs.

To explore the dynamic effects of the evolution of the Spike in humans, we examine asymmetry with these new potentially adaptive sites, namely the low EP (CAP) characteristic mutation sites observed in the Delta variant, the widely dominant variant from December 2021 to January 2022 (Thye et al. 2021), and the Omicron variant, a highly transmissible variant whose lineages have remained dominant since January 2022) (Kim et al. 2021) (Figure 4). This analysis revealed a mechanism similar to that for the CAPs in the

reference protein (Figure 2), as the open-chain binding interface is also allosterically controlled by these potentially new adaptive sites. Regarding this, we see that the asymmetry is much more pronounced in observed mutations of Omicron variants suggesting that these new mutations have a stronger power in controlling the dynamics of open chain hACE2 binding interface compared to those observed in Delta variants. We can speculate that the difference in virulence and infection rates between Omicron and Delta (Earnest et al. 2022; Bager et al. 2021; Sheikh et al. 2021; Twohig et al. 2022;(Houhamdi et al. 2022; Menni et al. 2022) might be due to these specific CAPs within each variant and their differences in allosterically controlling the dynamics of open RBD binding sites as observed in the DCI_{asym} analysis.

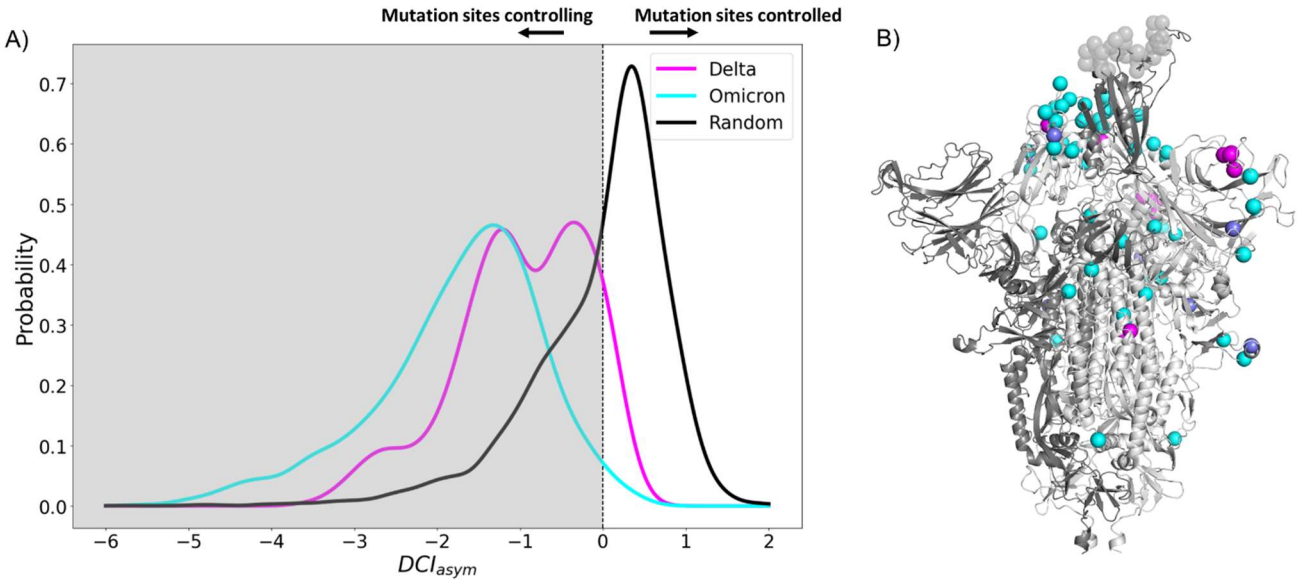

Figure 4. (A) DCI asymmetry with low EP characteristic mutation sites of Delta or Omicron strains in the closed chains and the binding interface of RBD in the open chain. Delta displays a second peak closer to zero, suggesting that Delta mutation sites (M = -0.98, SD = 0.80) have less allosteric control over the hACE2 binding sites than Omicron mutation sites (M = -1.74, SD = 1.00) ($p < .001$). However, both sets of sites have far more control over hACE2 binding sites than expected, based on a random control group (M = 0.03, SD = 0.85) ($p < .001$). (B) S protein structure showing binding interface sites (transparent gray), Delta mutation sites (magenta), Omicron mutation sites (cyan), and sites mutated in both Omicron and Delta (Blue).

287 **Experimental results motivate the use of EpiScore within the SARS-CoV-2 Spike protein.**

288 The fact that the identified CAPs in the reference protein and the more recently evolved CAPs of Delta
289 and Omicron variants both show a high degree of control over the active sites begs the question: what is
290 the complex interaction between these previous and new CAP sites? Motivated by this concept, we
291 explore the interplay of mutational pairs to understand the effects of the specific amino acid backgrounds
292 associated with these two predominant variants. Some CAP sites in Delta and Omicron have already been
293 considered adaptive (Kemp et al. 2021; Kistler et al. 2022; Maher et al. 2022; Neher 2022).

294 It is well understood that the impact of even a single mutation to a protein sequence can sometimes
295 dramatically alter the biophysical behavior of the system. However, the mechanistic impact of point
296 mutations can only be fully understood when the sequence background upon which it is made is
297 accounted for. This means that, in the case of strains with multiple mutations, the interplay between
298 mutated positions will ultimately impact a protein as an aggregate behavior, where the presence of
299 previous mutations may strongly (or weakly) influence some mutations. This concept of non-additivity is
300 known as epistasis. In fact, studies of evolutionary pathways of mutations have suggested that a majority
301 of the mutations have a second or a higher order epistasis among them (Bershtein et al. 2006). Nature
302 exploits this higher order complex relationship between the mutations to evolve their function.

303 To computationally capture and interpret the pairwise effects of mutations, we have developed an in-
304 house computational tool called EpiScore (Figure 5A). Here, we evaluate how a given position pair *i j* may
305 affect other critical positions *k* of the protein. EpiScore is the relative coupling strength to a position *k*
306 when positions *i* and *j* are perturbed *simultaneously* compared to the average dynamic coupling strength
307 of *i* to *k* and *j* to *k.* EpiScore has previously been used successfully to capture overarching trends in GB1
308 deep mutational scan data as well as specific instances of the development of antibiotic resistance in
309 various enzymatic systems (Campitelli and Ozkan 2020). An EpiScore of 1 indicates perfect coupling
310 additivity, and deviations from this value represent non-additive behavior between position pairs and

functionally important sites. Prior EpiScore work has shown a difference in EpiScore between the sites of compensatory and non-compensatory mutations, where both yield distributions with peaks around 1, but non-compensatory mutations show higher deviation in their EpiScore distribution (Ose, Campitelli, et al. 2022).

Many studies have confirmed epistasis between residues within the S protein (Moulana et al. 2022a; Starr, Greaney, Hannon, et al. 2022; Moulana et al. 2023; Witte et al. 2023). These epistatic residues can have various effects on hACE2 or antibody binding. To further motivate our use of EpiScore within SARS-CoV-2, we calculate the EpiScore (Figure 5B) of a set of mutation pairs used by Moulana et al. (Nature comm 2022) and compare our results to quantified epistatic effects determined by the experimental hACE2 binding affinity of "first-order" single mutation variants compared to "second-order" mutation pair. Our EpiScore results and the experimentally determined epistasis have a reasonable similarity. Both methods captured highly epistatic behavior among residues 493, 496, 498, 501, and 505, as well as a lack of epistatic behavior for residues 339, 371, 373, and 375.

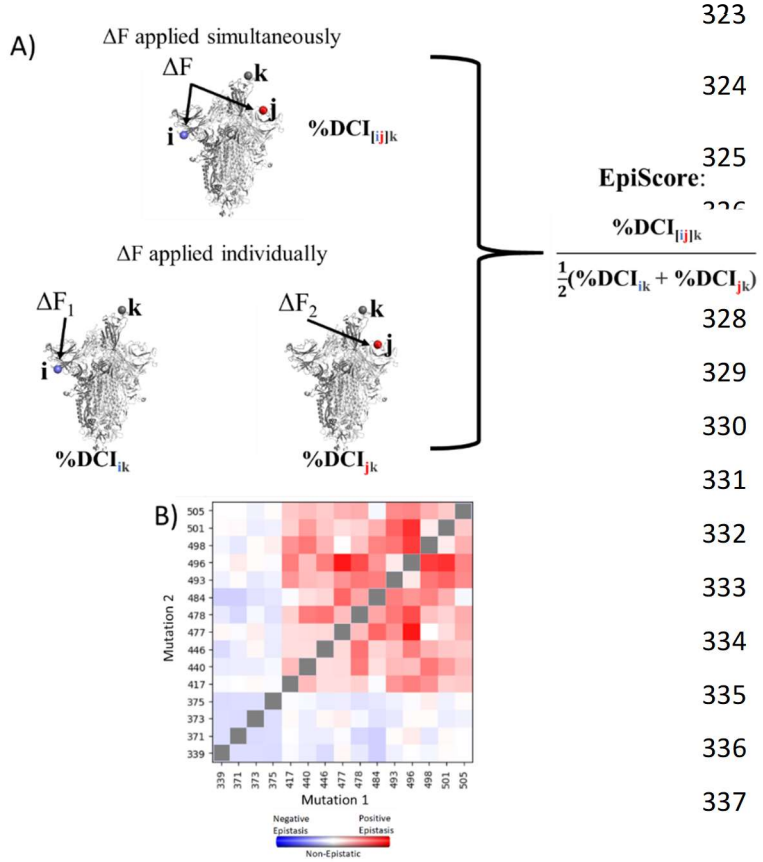

Figure 5. (A) Schematic representation of cross-chain EpiScore, describing i, j, in chain B and C respectively and its impact in RBD binding position k in the open RBD conformer chain A. (B) Colors indicate EpiScore values for given mutation pairs, averaged over hACE2 binding sites. Cross-chain residue pairs in the upper right tend to be highly epistatic, similar to pairwise second-order interaction coefficients from Moulana et al. (Nature comm 2022).

338 **Episcore highlights the epistatic relationship between the recent adaptive mutations in VOCs and the**
339 **CAPs of the Wuhan reference.**

340 Seeking further to understand the role of epistasis within S protein variants, we explored the possibility
341 of epistatic relationships between the CAPs of the Wuhan variant and the new CAPs in VOCs. Thus, we
342 computed the Episcore of these CAP positions in the closed RBD domains (i.e., chain B and C) with respect
343 to functional hACE2 binding interface sites of the open RBD domain chain (chain A) (Figure 5B) and
344 obtained Episcore distributions.

345

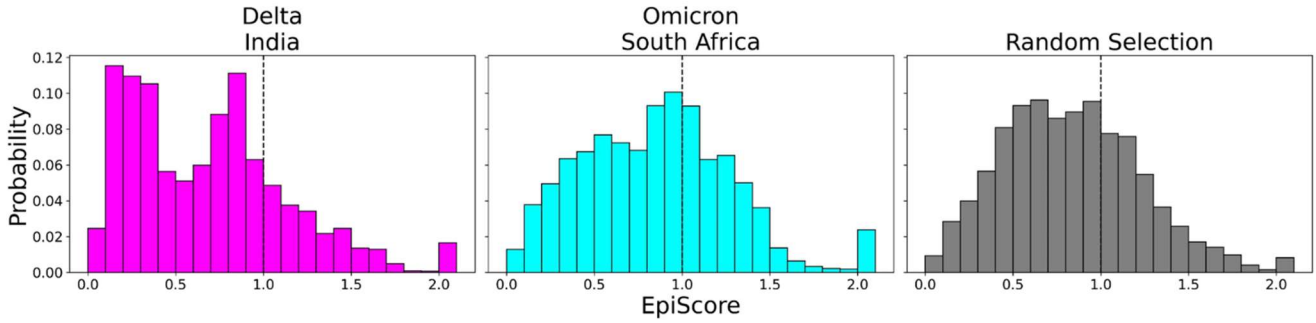

346

347 **Figure 6**. EpiScores with I = low EP Delta mutation sites (magenta), low EP Omicron mutation sites (Cyan),
348 and a random selection of sites (gray), j = low EP sites in the Wuhan variant, and k = the binding interface
349 of the open chain. EpiScores using sites of either variant (Delta: M = 0.70, SD = 0.50, Omicron M = 0.86,
350 SD = 0.46) are significantly different (p<.001) from a set of EpiScores using random sites (M = 0.84, SD =
351 0.41), but the distribution for Delta variants differs much more from the other two. EpiScores for other
352 variants can be found in Supplementary Figure S1.

353

354 To contrast these variants, Omicron (Figure 6, cyan) shows a high proportion of additive, potentially
355 compensatory, mutations compared to the Delta variant (Figure 6, magenta), with a peak centered on 1.
356 The comparatively more pathogenic Delta variant exhibited many non-additive, suspected non-
357 compensatory mutations with EpiScores below one. This again suggests that the cross-communication
358 between the open and closed chain of the S protein is important for regulating the function. Four out of

359 seven low EP Delta mutation sites used in this analysis often resulted in EpiScores below 1. Each of those
360 is found in the N-terminal domain (NTD) on or near the N3 loop and is implicated in antibody escape in
361 recent studies (Chi et al. 2020; Weisblum et al. 2020; Harvey, Carabelli, Jackson, Gupta, Thomson,
362 Harrison, Ludden, Reeve, Rambaut, COVID-19 Genomics UK (COG-UK) Consortium, et al. 2021; Klinakis et
363 al. 2021; Cantoni et al. 2022). The low EpiScores of NTD mutations suggest that they dampen the control
364 of Wuhan variant CAPs over the active site in addition to their effects on antibody binding. It is possible
365 that what the Delta variant gained in transmission rate also came with being more harmfully pathogenic
366 due in part to negatively epistatic interactions. It follows that the mutations leading to the development
367 of the Omicron strain were compensatory in nature, possibly leading to a lower pathogenicity and higher
368 effective immune escape, resulting in a higher transmission rate. It is worth noting that other variants
369 contain NTD mutations which result in low EpiScores, however the proportion of these mutations within
370 the set is considerably less than in Delta (Supplementary Figure S2).
371 One of the more notable similarities of generated EpiScore distributions is a tail of EpiScore values upward
372 of 2.0, indicating highly epistatic behavior. Interestingly, these tails are largely due to three different CAPs:
373 346R, 486F, and 498Q. Those residues are nearby one another within the protein structure and have been
374 reported to play a role in antibody binding, either being known antibody binding sites (346R and 486F) or
375 having received very high antibody accessibility scores (498Q) (Harvey, Carabelli, Jackson, Gupta,
376 Thomson, Harrison, Ludden, Reeve, Rambaut, COVID-19 Genomics UK (COG-UK) Consortium, et al. 2021;
377 Raghuvamsi et al. 2021). These observed high Episcore values also support the other studies that the
378 epistatic interactions between these CAPs and the mutations of the VOCs within the S protein are crucial
379 for maintaining binding affinity of hACE2 whilst evading immunity (Hong et al. 2022; Moulana et al. 2022b;
380 Starr, Greaney, Stewart, et al. 2022).
381 Viewing EpiScores of Delta and Omicron potentially adaptive mutation sites with only CAP site 486F (a
382 binding site for both hACE2 and antibodies) (Huang et al. 2020; Ali et al. 2021; Harvey, Carabelli, Jackson,

383 Gupta, Thomson, Harrison, Ludden, Reeve, Rambaut, COVID-19 Genomics UK (COG-UK) Consortium, et
384 al. 2021; Raghuvamsi et al. 2021) shows highly epistatic interactions at other hACE2 binding sites (Figure
385 6). However, within a recent and rapidly spreading subvariant of Omicron, XBB 1.5, we see a mutation of
386 F to S, a rare double nucleotide mutation, at site 486. This new variant has unprecedented immune escape
387 capabilities, resisting neutralizing antibodies almost entirely (Qu et al. 2023). EpiScores of other XBB 1.5
388 specific mutation sites with 486S are almost entirely greater than 1, showing an even higher degree of
389 epistasis with the binding sites of RBD (Figure 7). These results present a threefold importance for the
390 F486S mutation: Not only does this residue alter antibody (i.e., immune escape) and hACE2 binding by
391 directly modifying a binding site, but it may also be responsible for modifying hACE2 binding via epistatic
392 cooperation with other co-occurring mutations.

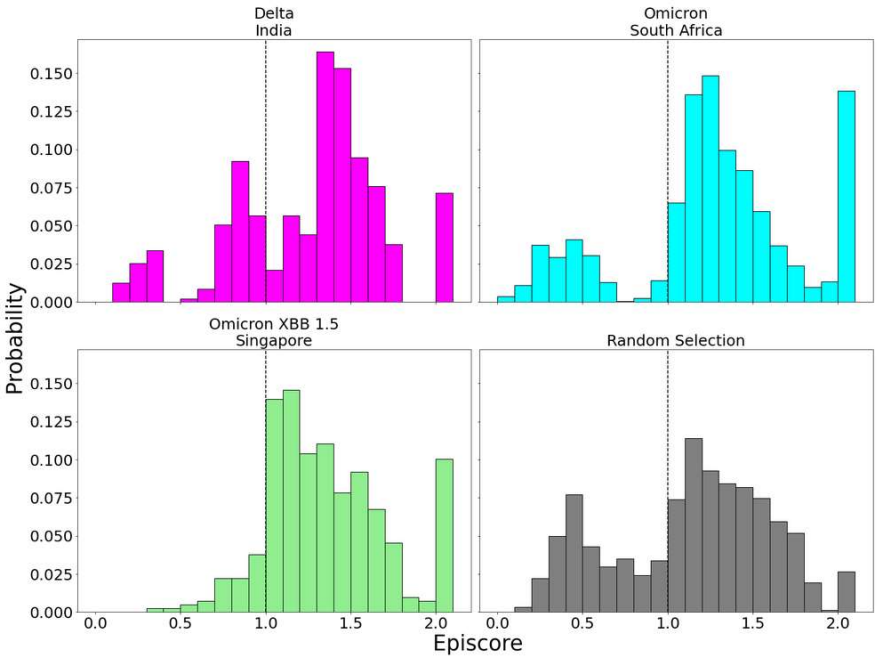

Figure 7. EpiScores with i = low EP Delta mutation sites (magenta), low EP Omicron mutation sites (Cyan), and a random selection of sites (gray), j = site 486, and k = the binding interface of the open chain. CAP and hACE2 and antibody binding site 486 displays epistasis with almost all XBB 1.5 variant sites at almost every hACE2

405
406 binding site (M = 1.40, SD = 0.46) and presents a significantly different profile from other variant sites (p
407 <.01). EpiScores involving 486 for other variants can be found in Supplementary Figure S1.
408

Change in flexibility of RBD binding site correlates with experimental binding affinities for Omicron and Omicron XBB variants.

Experimental studies have tracked hACE2 binding for different variants since the virus first spread (Ali et al. 2021; Barton et al. 2021; Ozono et al. 2021; Wu et al. 2022). Within the Omicron variant, for example, characteristic mutations on the RBD are shown to increase the overall binding affinity of the virus to the ACE2 receptor, which is suspected to allow it to spread more easily (Kim et al. 2021). Furthermore, the new Omicron XBB and Omicron XBB 1.5 variants contain additional mutations in the RBD and antibody binding residues, which may further impact their dynamics and interactions with the host.

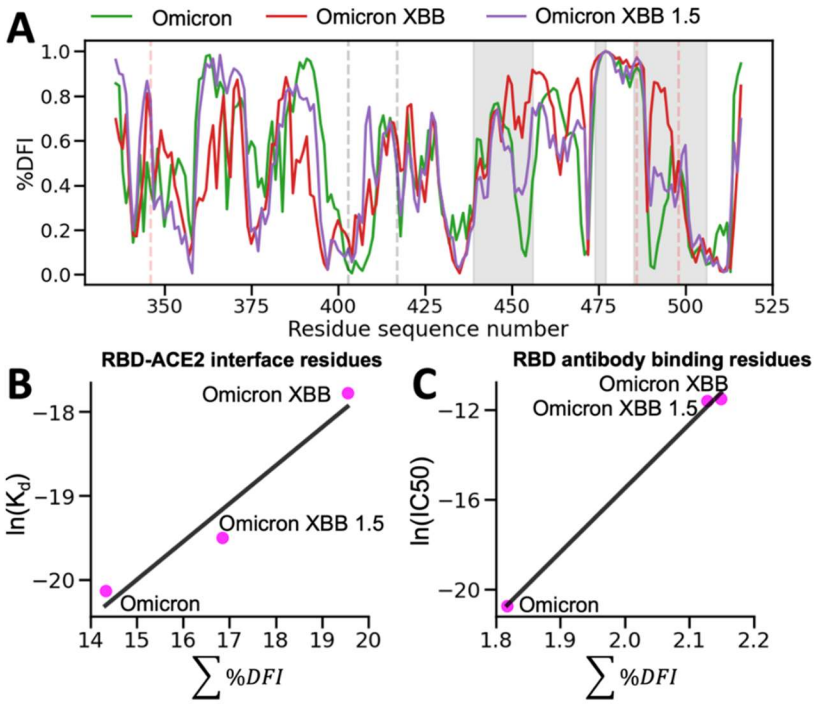

Figure 8. The %DFI calculations for variants Omicron, XBB, and XBB 1.5. (A) %DFI profile of the variants are plotted in the same panel. The grey shaded areas and dashed lines indicate the ACE2 binding regions, whereas the red dashed lines show the antibody binding residues. (B) The sum of %DFI values of RBD-ACE2 interface residues. The trend of total %DFI with the log of K_d values overlaps with the one seen with the experiments (R=0.97). (C) The RBD antibody binding residues are used to calculate the sum of %DFI. The ranking captured with the total %DFI agrees with the log of IC50 values from the experiments.

425 To gain deeper insights into the impact of dynamics on the binding affinity of hACE2 and antibodies with
426 the recent Omicron XBB variants, we conducted molecular dynamics (MD) simulations. By analyzing the
427 resulting trajectories, we investigated how these mutations influence the flexibility and rigidity of the RBD
428 and antibody binding residues, consequently affecting their binding affinity and potential for immune
429 evasion (Figure 8). To understand the overall flexibility changes, we measured the sum of DFI of the ACE2
430 binding residues, as well as the sum of DFI of the antibody binding residues, calculated from the MD
431 trajectories and compared then with experimental viral binding (disassociation constants) and immunity
432 evasion antibody IC50 values (Yue et al. 2023).
433 This investigation elucidated the impact of mutations in the receptor-binding domain (RBD) and antibody
434 binding residues on the binding affinity of the S protein and immune evasion by modulating their flexibility
435 and rigidity (Figure 8A). The Omicron XBB variant exhibits heightened flexibility in hACE2 and antibody
436 binding residues, reducing infectivity and enhancing immune evasion. Conversely, the Omicron XBB 1.5
437 variant induces distinct dynamics in these regions, rendering the RBD-ACE2 interface more rigid while
438 increasing flexibility in antibody binding residues. These effects indicate that Omicron XBB1.5 retains its
439 antibody escape capabilities while regaining ACE2 binding affinity comparable to previous Omicron
440 variants, in accordance with experimental findings (Yue et al. 2023). These findings suggest that mutations
441 in the RBD and antibody binding residues can have complex effects on the dynamics of the protein and,
442 ultimately, on the virus's ability to infect and evade the host immune system through an alteration of
443 biding site dynamics.
444

445 **Conclusion:**

446 We analyzed the evolutionary trajectory of the CoV-2 S protein in humans to understand the dynamic
447 and epistatic interactions of the mutations defining specific VOCs within the S protein. We first obtain
448 the phylogenetic tree of the COV-2 S protein and identify the sites of certain recent mutations known as

449 candidate adaptive polymorphisms (CAPs). CAPs are considered adaptive because mutations rarely
450 tolerated in closely related sequences have suddenly become fixed, implying a degree of functional
451 importance or evolution (Liu et al. 2016). In addition, our earlier work has shown that CAPS can also be
452 compensatory as multiple CAPs may dynamically compensate for one another, changing the dynamic
453 landscape and allowing for different mutations (Ose, Campitelli, et al. 2022). We then explored the
454 mechanistic insights and epistatic relationship between the observed mutations in different VOCs and
455 the CAP sites, and, particularly, the relationship between CAP sites and the functionally critical RBD
456 domain using our dynamic coupling analysis (Kumar, A., Glembo, T.J., Ozkan, S.B. 2015b).

457 We find a mechanistic pattern in the S protein evolution that is common amongst previously studied
458 systems, where allosteric sites exert control over the dynamics of the active site, and mutations of these
459 allosteric sites modulate function. Within the S protein, these critical regulatory sites are CAPs and VOC-
460 defining new putative adaptive mutations. However, this regulation is significantly less in Delta-defining
461 mutations than in the Omicron variant. We speculate that this may cause some differences in behavior
462 between the strains. Simply looking at the connection between hACE2 binding and pathogenicity, we
463 know that the Omicron variant is less pathogenic and has a lower binding affinity (Wu et al. 2022) than
464 previous variants. Our dynamics analysis provides a mechanistic insight where the Omicron defining
465 sites have greater control over the active sites than the Delta variant, and compensate for the functional
466 advantage of CAPs, thus, the greatest infectivity may not be a coincidence.

467 Specifically, we find that the interactions between CAP sites and VOC-defining mutations show
468 fingerprints of non-compensatory dynamics within the Delta variant. In contrast, mutations leading to
469 the Omicron variant are largely compensatory, driving critical dynamical behavior closer to the patterns
470 observed within the wild-type. These interactions may drive observed behavior similar between the
471 reference and Omicron strains yet differ in the delta strain, such as the severity of infection as evidenced
472 by hospitalization rates (Houhamdi et al. 2022; Menni et al. 2022).

473 Long-ranged interactions between different sites within a given protein is critically important for protein
474 function (Peters and Lively 1999; Bershtein et al. 2006; Collins et al. 2006; Ekeberg et al. 2013; Levy et al.
475 2017; Harrigan et al. 2018; Otten et al. 2018; Rojas Echenique et al. 2019; Shimagaki and Weigt 2019; de
476 la Paz et al. 2020; Rizzato et al. 2020; Yang et al. 2020; Bisardi et al. 2022) and for the CoV-2 S protein in
477 particular (Zeng et al. 2020; Castiglione et al. 2021; Dong et al. 2021; Garvin et al. 2021; Nielsen et al.
478 2022; Ramarao-Milne et al. 2022; Rochman et al. 2022; Rodriguez-Rivas et al. 2022). By showing dynamic
479 differences between the interactions of CAPs, which have likely played a major role in allowing the virus
480 to infect human hosts, the binding site, and the characteristic mutations of dominant Delta and Omicron
481 strains, we see a "fine-tuning" of protein behavior. As variants continue to evolve, Omicron sub-variants
482 are of growing concern due in large part to further increased immune evasion (Callaway 2022; Wang, Guo,
483 et al. 2022; Wang, Iketani, et al. 2022), and we observe that the new mutations observed in antibody
484 binding sites yield more epistatic interaction with the CAPs. In addition to supporting previous dynamic
485 research on the S protein, this analysis provides the insight that CAP sites are of continued importance to
486 protein function and should be given special attention when considering the impact of future mutations.
487

488 **Methods**

489

490 **Dynamic Flexibility and Dynamic Coupling**

491 The Dynamic Flexibility Index utilizes a Perturbation Response Scanning technique that combines the Elas-
492 tic Network Model (ENM) and Linear Response Theory (LRT) (Gerek and Ozkan 2011; Nevin Gerek, Z.,
493 Kumar, S., Banu Ozkan, S. 2013). In ENM, the protein is considered as a network of beads at Cα positions
494 interacting with each other via a harmonic spring potential. Using LRT, Δ**R** is calculated as the fluctuation
495 response vector of residue *j* due to unit force's **F** perturbation on residue *i,* averaged over multiple unit
496 force directions to simulate an isotropic perturbation.

$$[\Delta \mathbf{R}]_{3N\times 1} = [\mathbf{H}]^{-1}_{3N\times 3N}[\mathbf{F}]_{3N\times 1} \tag{1}$$

H is the Hessian, a 3N × 3N matrix that can be constructed from 3-D atomic coordinate information and is composed of the second derivatives of the harmonic potential with respect to the components of the position's vectors of length 3N. The hessian inverse in this equation may be replaced with the covariance matrix **G** obtained from MD simulations as follows.

$$[\Delta \mathbf{R}]_{3N\times 1} = [\mathbf{G}]_{3N\times 3N}[\mathbf{F}]_{3N\times 1} \tag{2}$$

MD simulations were used to obtain the DFI profiles of Omicron, Omicron XBB, and Omicron XBB 1.5. In order to obtain DFI, each position in the structure was perturbed sequentially to generate a Perturbation Response Matrix ***A***

$$\mathbf{A}_{N\times N} = \begin{bmatrix} |\Delta R^1|_1 & \cdots & |\Delta R^N|_1 \\ \vdots & \ddots & \vdots \\ |\Delta R^1|_N & \cdots & |\Delta R^N|_N \end{bmatrix} \tag{3}$$

where $|\Delta R^j|_i = \sqrt{\langle(\Delta R)^2\rangle}$ is the magnitude of fluctuation response at position *i* due to perturbations at position *j. T*he DFI value of position *i* is then treated as the displacement response of position *i* relative to the net displacement response of the entire protein, which is calculated by sequentially perturbing each position in the structure.

519 $$\mathrm{DFI_i} = \frac{\sum_{j=1}^{N} \left|\Delta R^j\right|_i}{\sum_{i=1}^{N} \sum_{j=1}^{N} \left|\Delta R^j\right|_i}$$

518 (4)

520 It is also often useful to quantify position flexibility relative to the flexibility ranges unique to individual
521 structures. To that end, DFI can be presented as a percentile rank, %DFI. All %DFI calculations present in
522 this work used the DFI value of every residue of the full spike structure for ranking. The DFI parameter can
523 be considered a measure of a given amino acid position's ability to explore its local conformational space.

524

525 **Dynamic Coupling Index**

526 Similar to DFI, the dynamic coupling index (DCI) (Larrimore et al. 2017; Kumar, A., Glembo, T.J., Ozkan,
527 S.B. 2015b) also utilizes Perturbation Response Scanning with the Elastic Network Model and Linear
528 Response Theory. DCI captures the strength of displacement response of a given position *i* upon
529 perturbation to a single functionally important position (or subset of positions) *j*, relative to the average
530 fluctuation response of position *i* when all of the positions within a structure are perturbed.

531

534 $$\mathrm{DCI_{ji}} = \frac{\sum_{j}^{N_{functional}} \left|\Delta R^j\right|_i / N_{functional}}{\sum_{j=1}^{N} \left|\Delta R^j\right|_i / N}$$

532 (5)

533 When only positional pairs are concerned, this expression reduces to:

535

537 $$\mathrm{DCI_{ji}} = \frac{\left|\Delta R^j\right|_i}{\sum_{j=1}^{N} \left|\Delta R^j\right|_i / N}$$

536 (6)

538 As such, this parameter represents a measure of the dynamic coupling between *i* and *j* upon a
539 perturbation to *j*. As with DFI, DCI_{ji} can also be presented as a percentile-ranked $\%DCI_{ji}$.

540 One of the most important aspects of DCI is that the entire network of interactions is explicitly included
541 in subsequent calculations without the need for dimensionality reduction techniques. If one considers
542 interactions such as communication directionality or dynamic coupling regulation between position pairs
543 as inherent properties of an anisotropic interaction network, it is critical to include the interactions of the
544 entire network to accurately model the effect one residue can have on another.

545 Here, we present two further extensions of DCI which allow us to uniquely model coupling directionality
546 and epistatic effects: DCI_{asym} and EpiScore, respectively. Interestingly, we can capture asymmetry between
547 different residues within a protein through DCI, as a coupling in and of itself is asymmetric within an ani-
548 sotropic network. That is, each amino acid has a set of positions to which it is highly coupled, and this
549 anisotropy in connections gives rise to unique differences in coupling between a given *i j* pair of amino
550 acids which do not have direct interactions (Figure 2A). DCI_{asym}, then, is simply DCI_{ij} (the normalized dis-
551 placement response of position *j* upon a perturbation to position *i*) − DCI_{ji} (Equation (7)). Using DCI_{asym} we
552 can determine a cause-effect relationship between the *i j* pair in terms of force/signal propagation be-
553 tween these two positions.

554

556 $$\mathrm{DCI_{asym}} = \mathrm{DCI_{ij}} - \mathrm{DCI_{ji}}$$
555 (7)

558 $$\%\mathrm{DCI_{asym}} = \%\mathrm{DCI_{ij}} - \%\mathrm{DCI_{ji}}$$
557 (8)

559 where a positive DCI_{asym} value indicates communication from position *i* to position *j*.

560 EpiScore can identify or describe potential non-additivity in substitution behavior between residue pairs.
561 This metric can capture the differences in a normalized perturbation response to a position *k* when a force
562 is applied at two residues *i* and *j* simultaneously versus the average additive perturbation response when
563 each residue *i*, *j*, is perturbed individually (Figure 5A, Equation 9).

566 $$\mathrm{EpiScore} = \frac{\%\mathrm{DCI}_{[ij]k}}{\frac{1}{2}\left(\%\mathrm{DCI}_{ik} + \%\mathrm{DCI}_{jk}\right)}$$

564

565 (9)

567

568 EpiScore values < 1 (> 1) indicate that the additive perturbations of positions *i* and *j* generates a greater
569 (lesser) response at position *k* than the effect of a simultaneous perturbation. This means that, when
570 treated with a simultaneous perturbation at both sites i and j, the displacement response of k is lower
571 (higher) than the average effect of individual perturbations to *i* and *j*, one at a time. As EpiScore is a linear
572 scale, the further the value from 1, the greater the effect described above.

573 **Molecular Dynamics (MD)**

574 The production simulations of the variants Omicron, Omicron XBB, and Omicron XBB 1.5 were generated
575 using the AMBER software package. The mutations in the variants were modeled using PYMOL taking the
576 template as PDB 6M0J. The initial input proteins were parametrized utilizing the ff14SB force field (Maier
577 et al. 2015). To ensure adequate solvation of the protein, the solvation box was defined to encompass the
578 protein, maintaining a minimum distance of 16Å from the protein to the box edges, utilizing the explicit
579 TIP3P water model (Sun 1995). The neutralization of the solvated system was achieved through the addi-
580 tion of sodium and chloride ions. The system was subjected to a steepest descent algorithm for 11000

581 steps for minimization purposes. The minimized system was then heated to 300K and subjected to a con-
582 stant number of particles, pressure, and temperature ensemble (NPT) production simulations. These sim-
583 ulations were conducted using the Langevin thermostat (Hünenberger 2005) and Berendsen barostat
584 (Berendsen et al. 1984). The hydrogens were constrained using the SHAKE algorithm (Pearlman et al.
585 1995). The production trajectories were simulated for 1µs at 300K and 1 bar.

586

587 **Data and Resource Availability**

588 The code to perform DFI and DCI analysis is available at https://github.com/SBOZKAN/DFI-DCI.
589 Molecular Dynamics data are available upon request. The mutation sites and EP values are contained in
590 the supporting information files as "Supplementary_mutation_info.csv". The alignment used to
591 generate EP values is also contained within the supporting information files as "EP_alignment.fas".
592 Protein Databank ID number 6VXX (Walls et al. 2020) was used for closed conformation DCI calculations.
593 6VSB (Wrapp et al. 2020) was used for DFI calculations, EpiScore calculations, and open conformation
594 DCI calculations. 6M0J (Lan et al. 2020) was used in molecular dynamics simulations of the RBD.

595 **Acknowledgements**

596 Funding was provided to N.J.O., P.C., T.M., and I.C.K. by the Gordon and Betty Moore Foundation (award
597 number AWD00034439) and to S.B.O. by the National Science Foundation (award numbers: 1715591
598 and 1901709) and the National Institutes of Health R01GM147635-01. S.K. acknowledges the National
599 Science Foundation (GCR 1934848) and the National Institutes of Health (GM139540) grants.

600 **References:**

601 Ali F, Kasry A, Amin M. 2021. The new SARS-CoV-2 strain shows a stronger binding affinity to ACE2 due
602 to N501Y mutant. *Med. Drug Discov.* 10:100086.

603 Amicone M, Borges V, Alves MJ, Isidro J, Zé-Zé L, Duarte S, Vieira L, Guiomar R, Gomes JP, Gordo I. 2022.
604 Mutation rate of SARS-CoV-2 and emergence of mutators during experimental evolution. *Evol.*
605 *Med. Public Health* 10:142–155.

606 Barton MI, MacGowan SA, Kutuzov MA, Dushek O, Barton GJ, van der Merwe PA. 2021. Effects of
607 common mutations in the SARS-CoV-2 Spike RBD and its ligand, the human ACE2 receptor on
608 binding affinity and kinetics. *eLife* 10:e70658.

609 Berendsen HJC, Postma JPM, van Gunsteren WF, DiNola A, Haak JR. 1984. Molecular dynamics with
610 coupling to an external bath. *J. Chem. Phys.* 81:3684–3690.

611 Berman, H.M., Westbrook, J., Feng, Z., Gilliland, G., Bhat, T.N., Weissig, H., Shindyalov, I.N., Bourne, P.E.
612 2000. The Protein Data Bank. *Nucleic Acids Res* 28:235–242.

613 Bershtein S, Segal M, Bekerman R, Tokuriki N, Tawfik DS. 2006. Robustness–epistasis link shapes the
614 fitness landscape of a randomly drifting protein. *Nature* 444:929–932.

615 Bhabha G, Ekiert DC, Jennewein M, Zmasek CM, Tuttle LM, Kroon G, Dyson HJ, Godzik A, Wilson IA,
616 Wright PE. 2013. Divergent evolution of protein conformational dynamics in dihydrofolate
617 reductase. *Nat. Struct. Mol. Biol.* 20:1243–1249.

618 Bisardi M, Rodriguez-Rivas J, Zamponi F, Weigt M. 2022. Modeling Sequence-Space Exploration and
619 Emergence of Epistatic Signals in Protein Evolution.Ozkan B, editor. *Mol. Biol. Evol.* 39:msab321.

620 Boni MF, Lemey P, Jiang X, Lam TT-Y, Perry BW, Castoe TA, Rambaut A, Robertson DL. 2020. Evolutionary
621 origins of the SARS-CoV-2 sarbecovirus lineage responsible for the COVID-19 pandemic. *Nat.*
622 *Microbiol.* 5:1408–1417.

623 Brister JR, Ako-adjei D, Bao Y, Blinkova O. 2015. NCBI Viral Genomes Resource. *Nucleic Acids Res.*
624 43:D571–D577.

625 Butler BM, Kazan IC, Kumar A, Ozkan SB. 2018. Coevolving residues inform protein dynamics profiles and
626 disease susceptibility of nSNVs.Jernigan RL, editor. *PLOS Comput. Biol.* 14:e1006626.

627 Cagliani R, Forni D, Clerici M, Sironi M. 2020. Computational Inference of Selection Underlying the
628 Evolution of the Novel Coronavirus, Severe Acute Respiratory Syndrome Coronavirus 2.Gallagher
629 T, editor. *J. Virol.* 94:e00411-20.

630 Callaway E. 2022. COVID 'variant soup' is making winter surges hard to predict. *Nature* 611:213–214.

631 Campbell, E., Kaltenbach, M., Correy, G., Carr, P., Porebski, B.T., Livingstone, E., Jurnou, L., Hyvönen, M.,
632 Buckle, A.M., Weik, M., et al. 2016. The role of protein dynamics in the evolution of new enzyme
633 function. *Nat Chem Biol*.

634 Campitelli P, Lu J, Ozkan SB. 2022. Dynamic allostery highlights the evolutionary differences between the
635 CoV-1 and CoV-2 main proteases. *Biophys. J.* 121:1483–1492.

636 Campitelli P, Modi T, Kumar S, Ozkan SB. The Role of Conformational Dynamics and Allostery in
637 Modulating Protein Evolution. *Annu. Rev. Biophys.* 49:267–288.

638 Campitelli P, Modi T, Kumar S, Ozkan SB. 2020a. The Role of Conformational Dynamics and Allostery in
639 Modulating Protein Evolution. *Annu. Rev. Biophys.* 49:267–288.

640 Campitelli P, Ozkan SB. 2020. Allostery and Epistasis: Emergent Properties of Anisotropic Networks.
641 *Entropy* 22:667.

642 Campitelli P, Swint-Kruse L, Ozkan SB. 2020b. Substitutions at Nonconserved Rheostat Positions
643 Modulate Function by Rewiring Long-Range, Dynamic Interactions.Wilke C, editor. *Mol. Biol.*
644 *Evol.* 38:201–214.

645 Cantoni D, Murray MJ, Kalemera MD, Dicken SJ, Stejskal L, Brown G, Lytras S, Coey JD, McKenna J,
646 Bridgett S, et al. 2022. Evolutionary remodelling of N-terminal domain loops fine-tunes SARS-
647 CoV -2 spike. *EMBO Rep.* [Internet] 23. Available from:
648 https://onlinelibrary.wiley.com/doi/10.15252/embr.202154322

649 Carabelli AM, Peacock TP, Thorne LG, Harvey WT, Hughes J, COVID-19 Genomics UK Consortium, De
650 Silva TI, Peacock SJ, Barclay WS, De Silva TI, et al. 2023. SARS-CoV-2 variant biology: immune
651 escape, transmission and fitness. *Nat. Rev. Microbiol.* [Internet]. Available from:
652 https://www.nature.com/articles/s41579-022-00841-7

653 Castiglione GM, Zhou L, Xu Z, Neiman Z, Hung C-F, Duh EJ. 2021. Evolutionary pathways to SARS-CoV-2
654 resistance are opened and closed by epistasis acting on ACE2.Hejnol A, editor. *PLOS Biol.*
655 19:e3001510.

656 Chan C-M, Woo PCY, Lau SKP, Tse H, Chen H-L, Li F, Zheng B-J, Chen L, Huang J-D, Yuen K-Y. 2008. Spike
657 Protein, S, of Human Coronavirus HKU1: Role in Viral Life Cycle and Application in Antibody
658 Detection. *Exp. Biol. Med.* 233:1527–1536.

659 Changeux J-P, Edelstein SJ. 2005. Allosteric Mechanisms of Signal Transduction. *Science* 308:1424–1428.

660 Chi X, Yan R, Zhang Jun, Zhang G, Zhang Y, Hao M, Zhang Z, Fan P, Dong Y, Yang Y, et al. 2020. A
661 neutralizing human antibody binds to the N-terminal domain of the Spike protein of SARS-CoV-
662 2. *Science* 369:650–655.

663 Collins SR, Schuldiner M, Krogan NJ, Weissman JS. 2006. A strategy for extracting and analyzing large-
664 scale quantitative epistatic interaction data. *Genome Biol.* 7:R63.

665 Damas J, Hughes GM, Keough KC, Painter CA, Persky NS, Corbo M, Hiller M, Koepfli K-P, Pfenning AR,
666 Zhao H, et al. 2020. Broad host range of SARS-CoV-2 predicted by comparative and structural
667 analysis of ACE2 in vertebrates. *Proc. Natl. Acad. Sci.* 117:22311–22322.

668 Deng X, Garcia-Knight MA, Khalid MM, Servellita V, Wang C, Morris MK, Sotomayor-González A, Glasner
669 DR, Reyes KR, Gliwa AS, et al. 2021. Transmission, infectivity, and antibody neutralization of an
670 emerging SARS-CoV-2 variant in California carrying a L452R spike protein mutation. Infectious
671 Diseases (except HIV/AIDS) Available from:
672 http://medrxiv.org/lookup/doi/10.1101/2021.03.07.21252647

673 Díaz-Salinas MA, Li Q, Ejemel M, Yurkovetskiy L, Luban J, Shen K, Wang Y, Munro JB. 2022.
674 Conformational dynamics and allosteric modulation of the SARS-CoV-2 spike. *eLife* 11:e75433.

675 Dicken SJ, Murray MJ, Thorne LG, Reuschl A-K, Forrest C, Ganeshalingham M, Muir L, Kalemera MD,
676 Palor M, McCoy LE, et al. 2021. Characterisation of B.1.1.7 and Pangolin coronavirus spike
677 provides insights on the evolutionary trajectory of SARS-CoV-2. Microbiology Available from:
678 http://biorxiv.org/lookup/doi/10.1101/2021.03.22.436468

679 Dong A, Zhao J, Griffin C, Wu R. 2021. The Genomic Physics of COVID-19 Pathogenesis and Spread. *Cells*
680 11:80.

681 Doshi U, Holliday MJ, Eisenmesser EZ, Hamelberg D. 2016. Dynamical network of residue–residue
682 contacts reveals coupled allosteric effects in recognition, catalysis, and mutation. *Proc. Natl.*
683 *Acad. Sci.* 113:4735–4740.

684 Dror RO, Dirks RM, Grossman JP, Xu H, Shaw DE. 2012. Biomolecular Simulation: A Computational
685 Microscope for Molecular Biology. *Annu. Rev. Biophys.* 41:429–452.

686 Ekeberg M, Lövkvist C, Lan Y, Weigt M, Aurell E. 2013. Improved contact prediction in proteins: Using
687 pseudolikelihoods to infer Potts models. *Phys. Rev. E* 87:012707.

688 Frost SDW, Magalis BR, Kosakovsky Pond SL. 2018. Neutral Theory and Rapidly Evolving Viral
689 Pathogens.Kumar S, editor. *Mol. Biol. Evol.* 35:1348–1354.

690 Garvin MR, Prates ET, Romero J, Cliff A, Machado Gazolla JGF, Pickholz M, Pavicic M, Jacobson D. 2021.
691 Rapid expansion of SARS-CoV-2 variants of concern is a result of adaptive epistasis. Evolutionary
692 Biology Available from: http://biorxiv.org/lookup/doi/10.1101/2021.08.03.454981

693 Gerek ZN, Ozkan SB. 2011. Change in Allosteric Network Affects Binding Affinities of PDZ Domains:
694 Analysis through Perturbation Response Scanning.Nussinov R, editor. *PLoS Comput. Biol.*
695 7:e1002154.

696 Gobeil SM-C, Janowska K, McDowell S, Mansouri K, Parks R, Manne K, Stalls V, Kopp MF, Henderson R,
697 Edwards RJ, et al. 2021. D614G Mutation Alters SARS-CoV-2 Spike Conformation and Enhances
698 Protease Cleavage at the S1/S2 Junction. *Cell Rep.* 34:108630.

699 Gobeil SM-C, Janowska K, McDowell S, Mansouri K, Parks R, Stalls V, Kopp MF, Manne K, Li D, Wiehe K,
700 et al. 2021. Effect of natural mutations of SARS-CoV-2 on spike structure, conformation, and
701 antigenicity. *Science* 373:eabi6226.

702 Goldman N. 1990. Maximum Likelihood Inference of Phylogenetic Trees, with Special Reference to a
703 Poisson Process Model of DNA Substitution and to Parsimony Analyses. *Syst. Zool.* 39:345.

704 Gur M, Taka E, Yilmaz SZ, Kilinc C, Aktas U, Golcuk M. 2020. Conformational transition of SARS-CoV-2
705 spike glycoprotein between its closed and open states. *J. Chem. Phys.* 153:075101.

706 Harrigan P, Madhani HD, El-Samad H. 2018. Real-Time Genetic Compensation Defines the Dynamic
707 Demands of Feedback Control. *Cell* 175:877-886.e10.

708 Harvey WT, Carabelli AM, Jackson B, Gupta RK, Thomson EC, Harrison EM, Ludden C, Reeve R, Rambaut
709 A, Consortium C-19 GU (COG-U, et al. 2021. SARS-CoV-2 variants, spike mutations and immune
710 escape. *Nat. Rev. Microbiol.* 19:409–424.

711 Harvey WT, Carabelli AM, Jackson B, Gupta RK, Thomson EC, Harrison EM, Ludden C, Reeve R, Rambaut
712 A, COVID-19 Genomics UK (COG-UK) Consortium, et al. 2021. SARS-CoV-2 variants, spike
713 mutations and immune escape. *Nat. Rev. Microbiol.* 19:409–424.

714 Henderson R, Edwards RJ, Mansouri K, Janowska K, Stalls V, Gobeil SMC, Kopp M, Li D, Parks R, Hsu AL,
715 et al. 2020. Controlling the SARS-CoV-2 spike glycoprotein conformation. *Nat. Struct. Mol. Biol.*
716 27:925–933.

717 Hoffmann M, Kleine-Weber H, Schroeder S, Krüger N, Herrler T, Erichsen S, Schiergens TS, Herrler G, Wu
718 N-H, Nitsche A, et al. 2020. SARS-CoV-2 Cell Entry Depends on ACE2 and TMPRSS2 and Is
719 Blocked by a Clinically Proven Protease Inhibitor. *Cell* 181:271-280.e8.

720 Hong Q, Han W, Li J, Xu S, Wang Yifan, Xu C, Li Z, Wang Yanxing, Zhang C, Huang Z, et al. 2022. Molecular
721 basis of receptor binding and antibody neutralization of Omicron. *Nature* 604:546–552.

722 Houhamdi L, Gautret P, Hoang VT, Fournier P, Colson P, Raoult D. 2022. Characteristics of the first 1119
723 SARS-CoV-2 Omicron variant cases, in Marseille, France, November−December 2021. *J. Med.*
724 *Virol.* 94:2290–2295.

725 Huang Y, Yang C, Xu X, Xu W, Liu S. 2020. Structural and functional properties of SARS-CoV-2 spike
726 protein: potential antivirus drug development for COVID-19. *Acta Pharmacol. Sin.* 41:1141–
727 1149.

728 Hünenberger PH. 2005. Thermostat Algorithms for Molecular Dynamics Simulations. In: Dr. Holm C, Prof.
729 Dr. Kremer K, editors. Advanced Computer Simulation. Vol. 173. Berlin, Heidelberg: Springer
730 Berlin Heidelberg. p. 105–149. Available from: http://link.springer.com/10.1007/b99427

731 Jackson CB, Farzan M, Chen B, Choe H. 2022. Mechanisms of SARS-CoV-2 entry into cells. *Nat. Rev. Mol.*
732 *Cell Biol.* 23:3–20.

733 Kazan IC, Mills JH, Ozkan SB. 2023. Allosteric regulatory control in dihydrofolate reductase is revealed by
734 dynamic asymmetry. *Protein Sci.* 32:e4700.

735 Kazan IC, Sharma P, Rahman MI, Bobkov A, Fromme R, Ghirlanda G, Ozkan SB. 2022. Design of novel
736 cyanovirin-N variants by modulation of binding dynamics through distal mutations. *eLife*
737 11:e67474.

738 Kemp SA, Collier DA, Datir RP, Ferreira IATM, Gayed S, Jahun A, Hosmillo M, Rees-Spear C, Mlcochova P,
739 Lumb IU, et al. 2021. SARS-CoV-2 evolution during treatment of chronic infection. *Nature*
740 592:277–282.

741 Keskin O, Bahar I, Jernigan RL, Beutler JA, Shoemaker RH, Sausville EA, Covell DG. 2000. Characterization
742 of anticancer agents by their growth inhibitory activity and relationships to mechanism of action
743 and structure. *Anticancer. Drug Des.* 15:79–98.

744 Khan A, Zia T, Suleman M, Khan T, Ali SS, Abbasi AA, Mohammad A, Wei D. 2021. Higher infectivity of the
745 SARS-CoV-2 new variants is associated with K417N/T, E484K, and N501Y mutants: An insight
746 from structural data. *J. Cell. Physiol.* 236:7045–7057.

747 Kim, H., Zou, T., Modi, C., Dörner, K., Grunkemeyer, T.J., Chen, L., Fromme, R., Matz, M. V., Ozkan, S.B.,
748 Wachter, R.M. 2015. A hinge migration mechanism unlocks the evolution of green-to-red
749 photoconversion in GFP-like proteins. *Structure* 23:34–43.

750 Kim Sinae, Nguyen TT, Taitt AS, Jhun H, Park H-Y, Kim S-H, Kim Y-G, Song EY, Lee Y, Yum H, et al. 2021.
751 SARS-CoV-2 Omicron Mutation Is Faster than the Chase: Multiple Mutations on Spike/ACE2
752 Interaction Residues. *Immune Netw.* 21:e38.

753 Kimura, Motoo. 1983. The neutral theory of molecular evolution. Cambridge University Press

754 Kirchdoerfer RN, Cottrell CA, Wang N, Pallesen J, Yassine HM, Turner HL, Corbett KS, Graham BS,
755 McLellan JS, Ward AB. 2016. Pre-fusion structure of a human coronavirus spike protein. *Nature*
756 531:118–121.

757 Kistler KE, Huddleston J, Bedford T. 2022. Rapid and parallel adaptive mutations in spike S1 drive clade
758 success in SARS-CoV-2. *Cell Host Microbe* 30:545-555.e4.

759 Klinakis A, Cournia Z, Rampias T. 2021. N-terminal domain mutations of the spike protein are structurally
760 implicated in epitope recognition in emerging SARS-CoV-2 strains. *Comput. Struct. Biotechnol. J.*
761 19:5556–5567.

762 Kolbaba-Kartchner B, Kazan IC, Mills JH, Ozkan SB. 2021. The Role of Rigid Residues in Modulating TEM-1
763 β-Lactamase Function and Thermostability. *Int. J. Mol. Sci.* 22:2895.

764 Kumar, A., Glembo, T.J., Ozkan, S.B. 2015b. The Role of Conformational Dynamics and Allostery in the
765 Disease Development of Human Ferritin. *Biophys J* 109:1273–1281.

766 Kumar S, Stecher G, Li M, Knyaz C, Tamura K. 2018. MEGA X: Molecular Evolutionary Genetics Analysis
767 across Computing Platforms.Battistuzzi FU, editor. *Mol. Biol. Evol.* 35:1547–1549.

768 Kumar S, Tao Q, Weaver S, Sanderford M, Caraballo-Ortiz MA, Sharma S, Pond SLK, Miura S. 2021. An
769 Evolutionary Portrait of the Progenitor SARS-CoV-2 and Its Dominant Offshoots in COVID-19
770 Pandemic.Yeager M, editor. *Mol. Biol. Evol.* 38:3046–3059.

771 Kuzmanic A, Bowman GR, Juarez-Jimenez J, Michel J, Gervasio FL. 2020. Investigating Cryptic Binding
772 Sites by Molecular Dynamics Simulations. *Acc. Chem. Res.* 53:654–661.

773 Labbadia J, Morimoto RI. 2015. The Biology of Proteostasis in Aging and Disease. *Annu. Rev. Biochem.*
774 84:435–464.

775 Laiton-Donato K, Franco-Muñoz C, Álvarez-Díaz DA, Ruiz-Moreno HA, Usme-Ciro JA, Prada DA, Reales-
776 González J, Corchuelo S, Herrera-Sepúlveda MT, Naizaque J, et al. 2021. Characterization of the
777 emerging B.1.621 variant of interest of SARS-CoV-2. *Infect. Genet. Evol.* 95:105038.

778 Lan J, Ge J, Yu J, Shan S, Zhou H, Fan S, Zhang Q, Shi X, Wang Q, Zhang L, et al. 2020. Structure of the
779 SARS-CoV-2 spike receptor-binding domain bound to the ACE2 receptor. *Nature* 581:215–220.

780 Larrimore KE, Kazan IC, Kannan L, Kendle RP, Jamal T, Barcus M, Bolia A, Brimijoin S, Zhan C-G, Ozkan SB,
781 et al. 2017. Plant-expressed cocaine hydrolase variants of butyrylcholinesterase exhibit altered
782 allosteric effects of cholinesterase activity and increased inhibitor sensitivity. *Sci. Rep.* 7:10419.

783 Levy RM, Haldane A, Flynn WF. 2017. Potts Hamiltonian models of protein co-variation, free energy
784 landscapes, and evolutionary fitness. *Curr. Opin. Struct. Biol.* 43:55–62.

785 Liu L, Tamura K, Sanderford M, Gray VE, Kumar S. 2016. A Molecular Evolutionary Reference for the
786 Human Variome. *Mol. Biol. Evol.* 33:245–254.

787 Liu Xueyan, Liu Xuan, Zhou J, Dong Y, Jiang Wen, Jiang Wenqing. 2022. Rampant C-to-U deamination
788 accounts for the intrinsically high mutation rate in SARS-CoV-2 spike gene. *RNA* 28:917–926.

789 Liu Y, Bahar I. 2012. Sequence Evolution Correlates with Structural Dynamics. *Mol. Biol. Evol.* 29:2253–
790 2263.

791 Ma B, Nussinov R. 2016. Conformational footprints. *Nat. Chem. Biol.* 12:890–891.

792 Maguid S, Fernandez-Alberti S, Echave J. 2008. Evolutionary conservation of protein vibrational
793 dynamics. *Gene* 422:7–13.

794 Maguid S, Fernández-Alberti S, Parisi G, Echave J. 2006. Evolutionary Conservation of Protein Backbone
795 Flexibility. *J. Mol. Evol.* 63:448–457.

796 Maher MC, Bartha I, Weaver S, Di Iulio J, Ferri E, Soriaga L, Lempp FA, Hie BL, Bryson B, Berger B, et al.
797 2022. Predicting the mutational drivers of future SARS-CoV-2 variants of concern. *Sci. Transl.*
798 *Med.* 14:eabk3445.

799 Maier JA, Martinez C, Kasavajhala K, Wickstrom L, Hauser KE, Simmerling C. 2015. ff14SB: Improving the
800 Accuracy of Protein Side Chain and Backbone Parameters from ff99SB. *J. Chem. Theory Comput.*
801 11:3696–3713.

802 Markov PV, Ghafari M, Beer M, Lythgoe K, Simmonds P, Stilianakis NI, Katzourakis A. 2023. The evolution
803 of SARS-CoV-2. *Nat. Rev. Microbiol.* 21:361–379.

804 Menni C, Valdes AM, Polidori L, Antonelli M, Penamakuri S, Nogal A, Louca P, May A, Figueiredo JC, Hu C,
805 et al. 2022. Symptom prevalence, duration, and risk of hospital admission in individuals infected
806 with SARS-CoV-2 during periods of omicron and delta variant dominance: a prospective
807 observational study from the ZOE COVID Study. *The Lancet* 399:1618–1624.

808 Mikulska-Ruminska K, Shrivastava I, Krieger J, Zhang S, Li H, Bayır H, Wenzel SE, VanDemark AP, Kagan
809 VE, Bahar I. 2019. Characterization of Differential Dynamics, Specificity, and Allostery of
810 Lipoxygenase Family Members. *J. Chem. Inf. Model.* 59:2496–2508.

811 Millet JK, Whittaker GR. 2014. Host cell entry of Middle East respiratory syndrome coronavirus after
812 two-step, furin-mediated activation of the spike protein. *Proc. Natl. Acad. Sci.* 111:15214–
813 15219.

814 Millet JK, Whittaker GR. 2015. Host cell proteases: Critical determinants of coronavirus tropism and
815 pathogenesis. *Virus Res.* 202:120–134.

816 Mishra SK, Jernigan RL. 2018. Protein dynamic communities from elastic network models align closely to
817 the communities defined by molecular dynamics.Zhang Y, editor. *PLOS ONE* 13:e0199225.

818 Modi T, Campitelli P, Kazan IC, Ozkan SB. 2021. Protein folding stability and binding interactions through
819 the lens of evolution: a dynamical perspective. *Curr. Opin. Struct. Biol.* 66:207–215.

820 Modi T, Ozkan S. 2018. Mutations Utilize Dynamic Allostery to Confer Resistance in TEM-1 β-lactamase.
821 *Int. J. Mol. Sci.* 19:3808.

822 Modi T, Risso VA, Martinez-Rodriguez S, Gavira JA, Mebrat MD, Van Horn WD, Sanchez-Ruiz JM, Banu
823 Ozkan S. 2021. Hinge-shift mechanism as a protein design principle for the evolution of β-
824 lactamases from substrate promiscuity to specificity. *Nat. Commun.* 12:1852.

825 Moulana A, Dupic T, Phillips AM, Chang J, Nieves S, Roffler AA, Greaney AJ, Starr TN, Bloom JD, Desai
826 MM. 2022a. Compensatory epistasis maintains ACE2 affinity in SARS-CoV-2 Omicron BA.1. *Nat.*
827 *Commun.* 13:7011.

828 Moulana A, Dupic T, Phillips AM, Chang J, Nieves S, Roffler AA, Greaney AJ, Starr TN, Bloom JD, Desai
829 MM. 2022b. Compensatory epistasis maintains ACE2 affinity in SARS-CoV-2 Omicron BA.1. *Nat.*
830 *Commun.* 13:7011.

831 Moulana A, Dupic T, Phillips AM, Chang J, Roffler AA, Greaney AJ, Starr TN, Bloom JD, Desai MM. 2023.
832 The landscape of antibody binding affinity in SARS-CoV-2 Omicron BA.1 evolution. *eLife*
833 12:e83442.

834 Neher RA. 2022. Contributions of adaptation and purifying selection to SARS-CoV-2 evolution. *Virus Evol.*
835 8:veac113.

836 Nevin Gerek, Z., Kumar, S., Banu Ozkan, S. 2013. Structural dynamics flexibility informs function and
837 evolution at a proteome scale. *Evol Appl*.

838 Nielsen BF, Li Y, Sneppen K, Simonsen L, Viboud C, Levin SA, Grenfell BT. 2022. Immune Heterogeneity
839 and Epistasis Explain Punctuated Evolution of SARS-CoV-2. Epidemiology Available from:
840 http://medrxiv.org/lookup/doi/10.1101/2022.07.27.22278129

841 Nussinov, R., Tsai, C.-J. 2013. Allostery in disease and in drug discovery. *Cell* 153:293–305.

842 O'Rourke KF, Gorman SD, Boehr DD. 2016. Biophysical and computational methods to analyze amino
843 acid interaction networks in proteins. *Comput. Struct. Biotechnol. J.* 14:245–251.

844 Ose NJ, Butler BM, Kumar A, Kazan IC, Sanderford M, Kumar S, Ozkan SB. 2022. Dynamic coupling of
845 residues within proteins as a mechanistic foundation of many enigmatic pathogenic missense
846 variants.Wallqvist A, editor. *PLOS Comput. Biol.* 18:e1010006.

847 Ose NJ, Campitelli P, Patel RP, Ozkan SB, Kumar S. 2022. Protein dynamics provide mechanistic insights
848 about the epistatic relationships among highly observed potentially adaptive missense variants.
849 *Biophys. J.* 121:456a.

850 Otten R, Liu L, Kenner LR, Clarkson MW, Mavor D, Tawfik DS, Kern D, Fraser JS. 2018. Rescue of
851 conformational dynamics in enzyme catalysis by directed evolution. *Nat. Commun.* 9:1314.

852 Ozono S, Zhang Y, Ode H, Sano K, Tan TS, Imai K, Miyoshi K, Kishigami S, Ueno T, Iwatani Y, et al. 2021.
853 SARS-CoV-2 D614G spike mutation increases entry efficiency with enhanced ACE2-binding
854 affinity. *Nat. Commun.* 12:848.

855 Patel R, Scheinfeldt LB, Sanderford MD, Lanham TR, Tamura K, Platt A, Glicksberg BS, Xu K, Dudley JT,
856 Kumar S. 2018. Adaptive Landscape of Protein Variation in Human Exomes.Yeager M, editor.
857 *Mol. Biol. Evol.* 35:2015–2025.

858 de la Paz JA, Nartey CM, Yuvaraj M, Morcos F. 2020. Epistatic contributions promote the unification of
859 incompatible models of neutral molecular evolution. *Proc. Natl. Acad. Sci.* 117:5873–5882.

860 Pearlman DA, Case DA, Caldwell JW, Ross WS, Cheatham III TE, DeBolt S, Ferguson D, Seibel G, Kollman
861 P. 1995. AMBER, a package of computer programs for applying molecular mechanics, normal
862 mode analysis, molecular dynamics and free energy calculations to simulate the structural and
863 energetic properties of molecules. *Comput Phys Commun* 91:1–41.

864 Peters AD, Lively CM. 1999. The Red Queen and Fluctuating Epistasis: A Population Genetic Analysis of
865 Antagonistic Coevolution. *Am. Nat.* 154:393–405.

866 Qu P, Faraone JN, Evans JP, Zheng Y-M, Carlin C, Anghelina M, Stevens P, Fernandez S, Jones D, Panchal
867 A, et al. 2023. Extraordinary Evasion of Neutralizing Antibody Response by Omicron XBB.1.5,
868 CH.1.1 and CA.3.1 Variants. Microbiology Available from:
869 http://biorxiv.org/lookup/doi/10.1101/2023.01.16.524244

870 Raghuvamsi PV, Tulsian NK, Samsudin F, Qian X, Purushotorman K, Yue G, Kozma MM, Hwa WY, Lescar J,
871 Bond PJ, et al. 2021. SARS-CoV-2 S protein:ACE2 interaction reveals novel allosteric targets. *eLife*
872 10:e63646.

873 Ramarao-Milne P, Jain Y, Sng LMF, Hosking B, Lee C, Bayat A, Kuiper M, Wilson LOW, Twine NA, Bauer
874 DC. 2022. Data-driven platform for identifying variants of interest in COVID-19 virus. *Comput.*
875 *Struct. Biotechnol. J.* 20:2942–2950.

876 Rehman S ur, Shafique L, Ihsan A, Liu Q. 2020. Evolutionary Trajectory for the Emergence of Novel
877 Coronavirus SARS-CoV-2. *Pathogens* 9:240.

878 Rizzato F, Coucke A, de Leonardis E, Barton JP, Tubiana J, Monasson R, Cocco S. 2020. Inference of
879 compressed Potts graphical models. *Phys. Rev. E* 101:012309.

880 Rochman ND, Faure G, Wolf YI, Freddolino PL, Zhang F, Koonin EV. 2022. Epistasis at the SARS-CoV-2
881 Receptor-Binding Domain Interface and the Propitiously Boring Implications for Vaccine
882 Escape.Diamond MS, editor. *mBio* 13:e00135-22.

883 Rochman ND, Wolf YI, Faure G, Mutz P, Zhang F, Koonin EV. 2021. Ongoing global and regional adaptive
884 evolution of SARS-CoV-2. *Proc. Natl. Acad. Sci.* 118:e2104241118.

885 Rodriguez-Rivas J, Croce G, Muscat M, Weigt M. 2022. Epistatic models predict mutable sites in SARS-
886 CoV-2 proteins and epitopes. *Proc. Natl. Acad. Sci.* 119:e2113118119.

887 Rojas Echenique JI, Kryazhimskiy S, Nguyen Ba AN, Desai MM. 2019. Modular epistasis and the
888 compensatory evolution of gene deletion mutants.Butler G, editor. *PLOS Genet.* 15:e1007958.

889 Saavedra HG, Wrabl JO, Anderson JA, Li J, Hilser VJ. 2018. Dynamic allostery can drive cold adaptation in
890 enzymes. *Nature* 558:324–328.

891 Saputri DS, Li S, van Eerden FJ, Rozewicki J, Xu Z, Ismanto HS, Davila A, Teraguchi S, Katoh K, Standley
892 DM. 2020. Flexible, Functional, and Familiar: Characteristics of SARS-CoV-2 Spike Protein
893 Evolution. *Front. Microbiol.* 11:2112.

894 Sekhar A, Kay LE. 2019. An NMR View of Protein Dynamics in Health and Disease. *Annu. Rev. Biophys.*
895 48:297–319.

896 Shang J, Wan Y, Luo C, Ye G, Geng Q, Auerbach A, Li F. 2020. Cell entry mechanisms of SARS-CoV-2. *Proc.*
897 *Natl. Acad. Sci.* 117:11727–11734.

898 Shimagaki K, Weigt M. 2019. Selection of sequence motifs and generative Hopfield-Potts models for
899 protein families. *Phys. Rev. E* 100:032128.

900 Shoemark DK, Oliveira ASF, Davidson AD, Berger I, Schaffitzel C, Mulholland AJ. 2022. Molecular
901 dynamics of spike variants in the locked conformation: RBD interfaces, fatty acid binding and
902 furin cleavage sites. Biochemistry Available from:
903 http://biorxiv.org/lookup/doi/10.1101/2022.05.06.490927

904 Singh D, Yi SV. 2021. On the origin and evolution of SARS-CoV-2. *Exp. Mol. Med.* 53:537–547.

905 Spinello A, Saltalamacchia A, Borišek J, Magistrato A. 2021. Allosteric Cross-Talk among Spike's Receptor-
906 Binding Domain Mutations of the SARS-CoV-2 South African Variant Triggers an Effective
907 Hijacking of Human Cell Receptor. *J. Phys. Chem. Lett.* 12:5987–5993.

908 Starr TN, Greaney AJ, Hannon WW, Loes AN, Hauser K, Dillen JR, Ferri E, Farrell AG, Dadonaite B,
909 McCallum M, et al. 2022. Shifting mutational constraints in the SARS-CoV-2 receptor-binding
910 domain during viral evolution. *Science* 377:420–424.

911 Starr TN, Greaney AJ, Stewart CM, Walls AC, Hannon WW, Veesler D, Bloom JD. 2022. Deep mutational
912 scans for ACE2 binding, RBD expression, and antibody escape in the SARS-CoV-2 Omicron BA.1
913 and BA.2 receptor-binding domains.Mok CKP, editor. *PLOS Pathog.* 18:e1010951.

914 Starr TN, Zepeda SK, Walls AC, Greaney AJ, Alkhovsky S, Veesler D, Bloom JD. 2022. ACE2 binding is an
915 ancestral and evolvable trait of sarbecoviruses. *Nature* 603:913–918.

916 Steinhauer DA. 1999. Role of Hemagglutinin Cleavage for the Pathogenicity of Influenza Virus. *Virology*
917 258:1–20.

Stevens AO, Kazan IC, Ozkan B, He Y. 2022. Investigating the allosteric response of the PICK1 PDZ domain to different ligands with all-atom simulations. *Protein Sci.* 31:e4474.

Sun PA Y, Kollman. 1995. Hydrophobic solvation of methane and nonbond parameters of the TIP3P water model. *J Comput Chem* 16:1164–1169.

Swint-Kruse L, Matthews KS, Smith PE, Pettitt BM. 1998. Comparison of Simulated and Experimentally Determined Dynamics for a Variant of the LacI DNA-Binding Domain, Nlac-P. *Biophys. J.* 74:413–421.

Sztain T, Ahn S-H, Bogetti AT, Casalino L, Goldsmith JA, Seitz E, McCool RS, Kearns FL, Acosta-Reyes F, Maji S, et al. 2021. A glycan gate controls opening of the SARS-CoV-2 spike protein. *Nat. Chem.* 13:963–968.

Tan ZW, Tee W-V, Samsudin F, Guarnera E, Bond PJ, Berezovsky IN. 2022. Allosteric perspective on the mutability and druggability of the SARS-CoV-2 Spike protein. *Structure* 30:590-607.e4.

Tang X, Wu C, Li X, Song Y, Yao X, Wu X, Duan Y, Zhang H, Wang Y, Qian Z, et al. 2020. On the origin and continuing evolution of SARS-CoV-2. *Natl. Sci. Rev.* 7:1012–1023.

Tay JH, Porter AF, Wirth W, Duchene S. 2022. The Emergence of SARS-CoV-2 Variants of Concern Is Driven by Acceleration of the Substitution Rate.Leitner T, editor. *Mol. Biol. Evol.* 39:msac013.

Teruel N, Mailhot O, Najmanovich RJ. 2021. Modelling conformational state dynamics and its role on infection for SARS-CoV-2 Spike protein variants.Dunbrack RL, editor. *PLOS Comput. Biol.* 17:e1009286.

Thye AY-K, Law JW-F, Pusparajah P, Letchumanan V, Chan K-G, Lee L-H. 2021. Emerging SARS-CoV-2 Variants of Concern (VOCs): An Impending Global Crisis. *Biomedicines* 9:1303.

Walls AC, Park Y-J, Tortorici MA, Wall A, McGuire AT, Veesler D. 2020. Structure, Function, and Antigenicity of the SARS-CoV-2 Spike Glycoprotein. *Cell* 181:281-292.e6.

Wang Q, Guo Y, Iketani S, Nair MS, Li Z, Mohri H, Wang M, Yu J, Bowen AD, Chang JY, et al. 2022. Antibody evasion by SARS-CoV-2 Omicron subvariants BA.2.12.1, BA.4 and BA.5. *Nature* 608:603–608.

Wang Q, Iketani S, Li Z, Liu Liyuan, Guo Y, Huang Y, Bowen AD, Liu M, Wang M, Yu J, et al. 2022. Alarming antibody evasion properties of rising SARS-CoV-2 BQ and XBB subvariants. *Cell*:S0092867422015318.

Weisblum Y, Schmidt F, Zhang F, DaSilva J, Poston D, Lorenzi JC, Muecksch F, Rutkowska M, Hoffmann H-H, Michailidis E, et al. 2020. Escape from neutralizing antibodies by SARS-CoV-2 spike protein variants. *eLife* 9:e61312.

Witte L, Baharani VA, Schmidt F, Wang Z, Cho A, Raspe R, Guzman-Cardozo C, Muecksch F, Canis M, Park DJ, et al. 2023. Epistasis lowers the genetic barrier to SARS-CoV-2 neutralizing antibody escape. *Nat. Commun.* 14:302.

953 Wrapp D, Wang N, Corbett KS, Goldsmith JA, Hsieh C-L, Abiona O, Graham BS, McLellan JS. 2020. Cryo-
954 EM structure of the 2019-nCoV spike in the prefusion conformation. *Science* 367:1260–1263.

955 Wrobel AG, Benton DJ, Xu P, Roustan C, Martin SR, Rosenthal PB, Skehel JJ, Gamblin SJ. 2020. SARS-CoV-
956 2 and bat RaTG13 spike glycoprotein structures inform on virus evolution and furin-cleavage
957 effects. *Nat. Struct. Mol. Biol.* 27:763–767.

958 Wu L, Zhou L, Mo M, Liu T, Wu C, Gong C, Lu K, Gong L, Zhu W, Xu Z. 2022. SARS-CoV-2 Omicron RBD
959 shows weaker binding affinity than the currently dominant Delta variant to human ACE2. *Signal*
960 *Transduct. Target. Ther.* 7:8.

961 Xue Q, Liu X, Pan W, Zhang A, Fu J, Jiang G. 2022. Computational Insights into the Allosteric Effect and
962 Dynamic Structural Features of the SARS-COV-2 Spike Protein. *Chem. – Eur. J.* [Internet] 28.
963 Available from: https://onlinelibrary.wiley.com/doi/10.1002/chem.202104215

964 Yang QE, MacLean C, Papkou A, Pritchard M, Powell L, Thomas D, Andrey DO, Li M, Spiller B, Yang W, et
965 al. 2020. Compensatory mutations modulate the competitiveness and dynamics of plasmid-
966 mediated colistin resistance in Escherichia coli clones. *ISME J.* 14:861–865.

967 Yue C, Song W, Wang L, Jian F, Chen X, Gao F, Shen Z, Wang Y, Wang X, Cao Y. 2023. Enhanced
968 transmissibility of XBB.1.5 is contributed by both strong ACE2 binding and antibody evasion.
969 Immunology Available from: http://biorxiv.org/lookup/doi/10.1101/2023.01.03.522427

970 Yurkovetskiy L, Wang X, Pascal KE, Tomkins-Tinch C, Nyalile TP, Wang Y, Baum A, Diehl WE, Dauphin A,
971 Carbone C, et al. 2020. Structural and Functional Analysis of the D614G SARS-CoV-2 Spike
972 Protein Variant. *Cell* 183:739-751.e8.

973 Zeng H-L, Dichio V, Rodríguez Horta E, Thorell K, Aurell E. 2020. Global analysis of more than 50,000
974 SARS-CoV-2 genomes reveals epistasis between eight viral genes. *Proc. Natl. Acad. Sci.*
975 117:31519–31526.

976 Zhang J, Cai Y, Xiao T, Lu J, Peng H, Sterling SM, Walsh RM, Rits-Volloch S, Zhu H, Woosley AN, et al.
977 2021. Structural impact on SARS-CoV-2 spike protein by D614G substitution. *Science* 372:525–
978 530.

979 Zhou T, Tsybovsky Y, Gorman J, Rapp M, Cerutti G, Chuang G-Y, Katsamba PS, Sampson JM, Schön A,
980 Bimela J, et al. 2020. Cryo-EM Structures of SARS-CoV-2 Spike without and with ACE2 Reveal a
981 pH-Dependent Switch to Mediate Endosomal Positioning of Receptor-Binding Domains. *Cell Host*
982 *Microbe* 28:867-879.e5.

983

984

985 **<u>Supplemental Figures</u>**

986

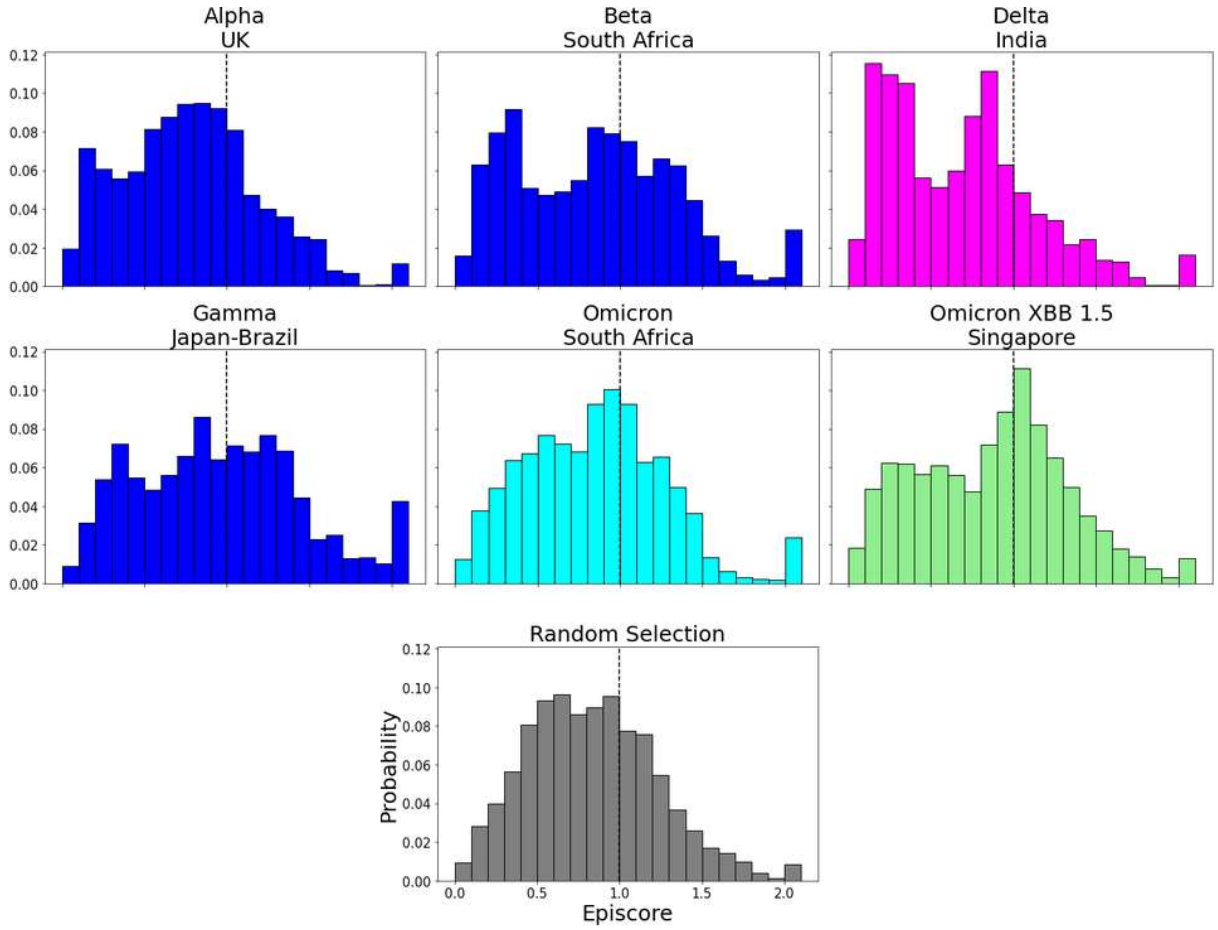

Supplementary figure S1. EpiScores with i = characteristic mutation sites, j = low EP sites, and k = the binding interface of the open chain. EpiScores using variant sites are significantly different ($p<.001$) from a set of EpiScores using random sites.

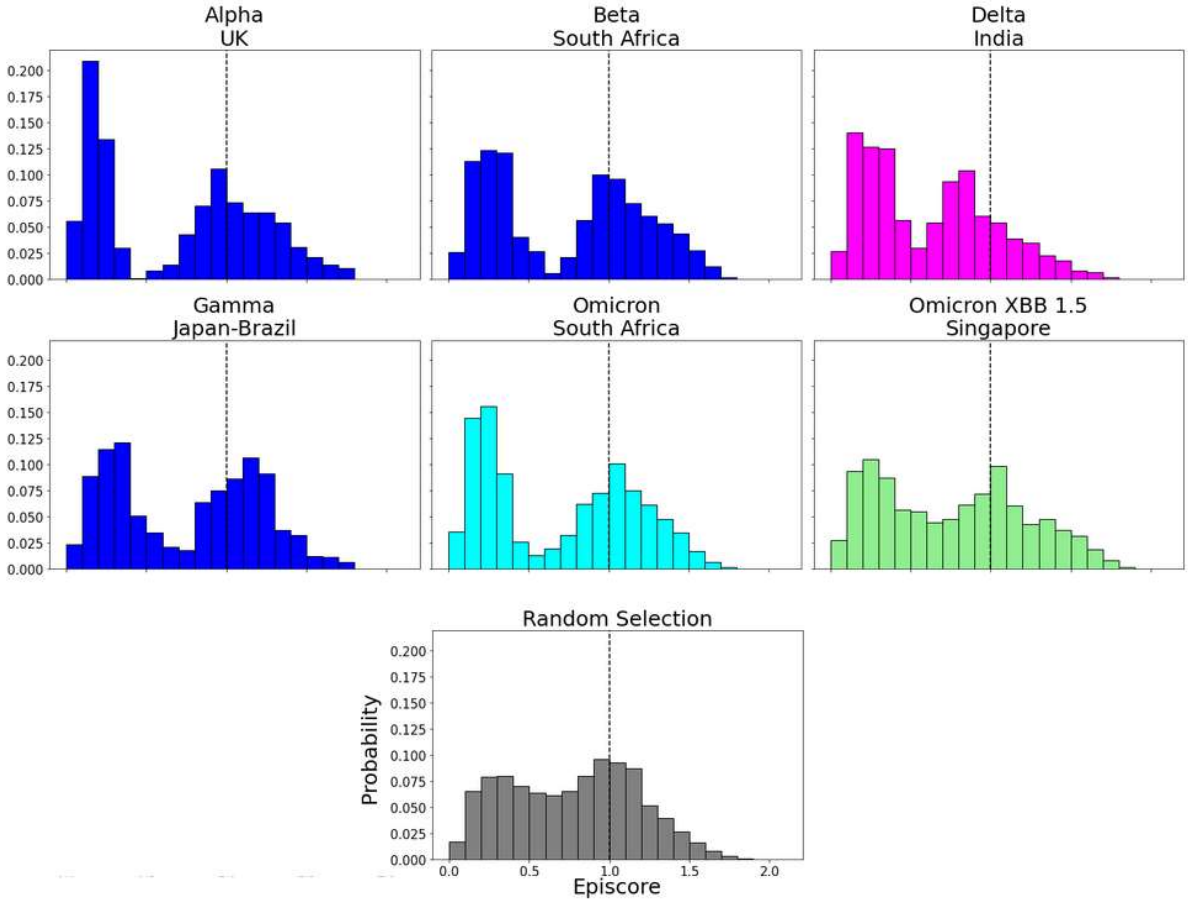

Supplementary figure S2. EpiScores with i = characteristic mutation sites within the NTD, j = low EP sites, and k = the binding interface of the open chain. NTD domain mutation sites result in markedly lower EpiScores compared to elsewhere.

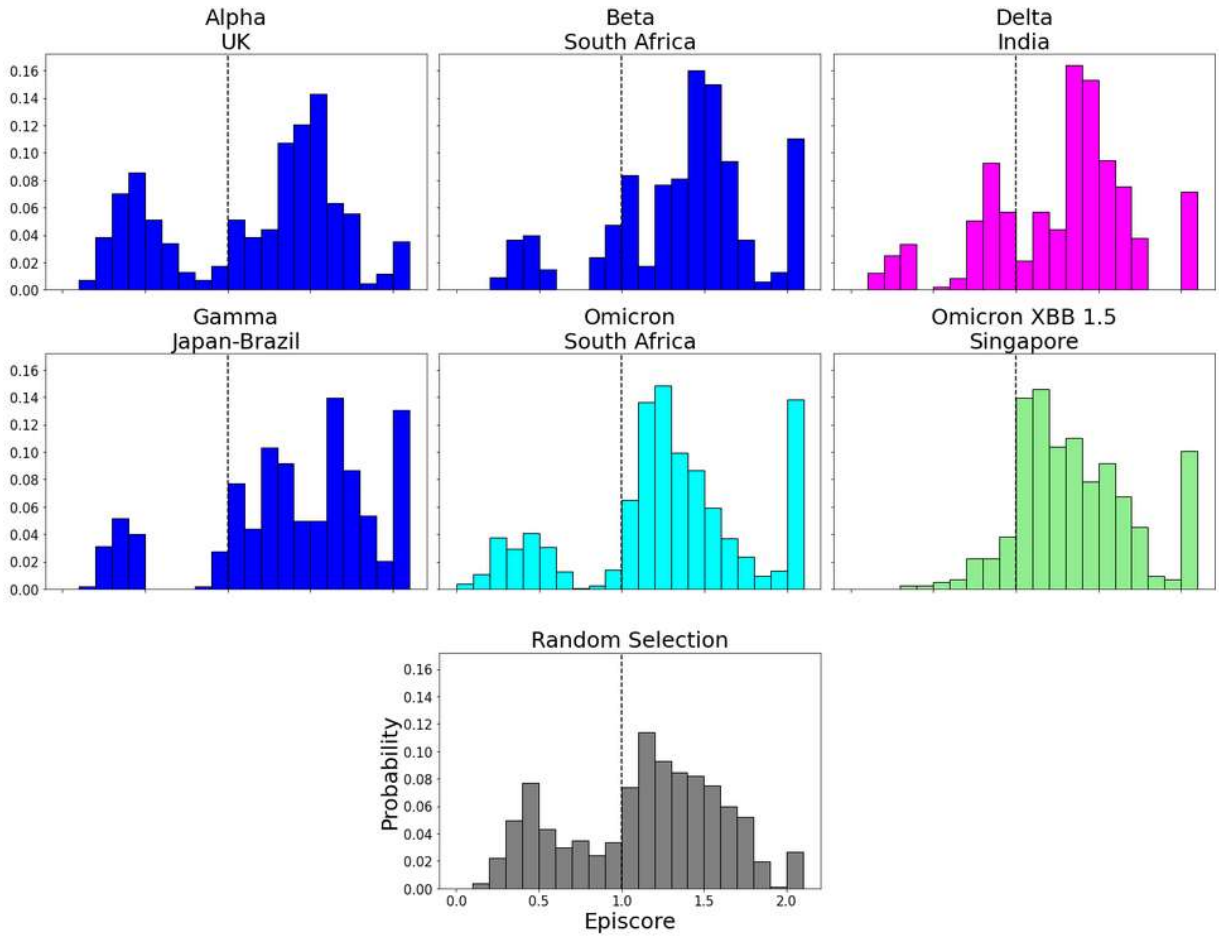

Supplementary figure S3. EpiScores with i = characteristic mutation sites, j = site 486, and k = the binding interface of the open chain. CAP and hACE2 and antibody binding site 486 displays epistasis with almost all XBB 1.5 variant sites at almost every hACE2 binding site. EpiScores using variant sites are significantly different ($p<.001$) from a set of EpiScores using random sites.